AR-009-961

DSTO-TN-0067

Finite Element Analysis of an F-111 Lower Wing Skin Fatigue Crack Repair

R.J. Callinan, S. Sanderson and D. Keeley

19970429 154

DEPARTMENT ◆ OF DEFENCE

DEFENCE SCIENCE AND TECHNOLOGY ORGANISATION

Finite Element Analysis of an F-111 Lower Wing Skin Fatigue Crack Repair

R.J.Callinan, S.Sanderson and D.Keeley

Airframes and Engines Division
Aeronautical and Maritime Research Laboratory

ABSTRACT

In this report a three dimensional finite element (F.E.) model has been developed for a structural detail in an F-111 lower wing skin. The location of interest is a fuel - flow groove in the lower wing skin where cracking had occurred in service on aircraft A8-145. Detailed models were developed for (i) un-cracked structure; (ii) the cracked structure and (iii) the repaired structure, using a bonded composite patch for the repair. The objective of this work is to validate the design analysis used by the RAAF, using an independent approach for the stress analysis. The F.E. model has been validated using strain gauge results from a full scale test wing. The results of the F.E. analysis are shown to compare favourably with closed form solutions used by the RAAF (RAAF Engineering Standard C5033) in the original design of the repair. Thus the present work provides a basis for confidence in the design procedures contained in RAAF Engineering Standard C5033.

RELEASE LIMITATION

Approved for Public Release

DEPARTMENT OF DEFENCE
◆
DEFENCE SCIENCE AND TECHNOLOGY ORGANISATION

Finite Element Analysis of an F-111 Lower Wing Skin Fatigue Crack Repair

Executive Summary

Following the discovery of a 48 mm fatigue crack in an Australian F-111 aircraft, the RAAF implemented a boron/epoxy composite repair, in which the design was based on closed form solutions using RAAF Engineering Standard C5033. Since primary structure was involved, the RAAF requested that the design analysis be validated by an independent method and a comprehensive structural testing program involving both static and fatigue loading. The objective of the present work being the validation of the design analysis using finite element analysis (F.E.) as the independent approach for the stress analysis.

In this report a three dimensional F.E. model has been developed for a structural detail in the F-111 lower wing skin which contains a fuel flow groove in which cracking has occurred. A detailed F.E. model has been developed for the un-cracked structure and validated by a static strain survey on a full scale test wing. This model has been extended to include a 48 mm crack, which provides a basis for residual strength calculations to be made. Finally, the adhesive and boron/epoxy composite repair has been added to the model, and has also been validated by strain gauge data.

The results obtained from these models compare favourably with closed form solutions used in the original RAAF design, (using C5033) and the present work provides a basis for the confidence in the design analysis of C5033. Furthermore, the results given here show that the static strength is restored and the crack growth rate is substantially reduced. The results from this analysis, together with the results from the extensive structural testing program, have substantiated this repair for the expected service life of the F-111.

Authors

R.J.Callinan
Airframes and Engines Division

Mr. R.J.Callinan is a senor research scientist and graduated from RMIT (Aero. Eng.) in 1969 and from Monash University in 1971 (Civil. Eng.) and completed a M.Eng. Sc. in 1981 at Melbourne University. His work has been in the areas of finite element analysis, fracture mechanics and structural mechanics of composite and bonded repairs, and military aircraft accident investigations. He has also been involved with design studies of low radar cross-section battlefield surveillance R.P.V.'s. In 1985 he was seconded to the USAF at Eglin AFB for 18 months, to carry out vulnerability studies on composite structures.

S.Sanderson
Airframes and Engines Division

Mr. Sanderson has worked at AMRL since 1981. He has developed flight data reduction & analysis software for Mirage, F-111 & F/A-18 projects. Several of these programs have been implemented by NAE for their data reduction in the IFOST project. Since 1992 Mr.Sanderson has been involved with the F.E. analysis of composite and bonded structures for F-111 & F/A-18.

D.Keeley
Airframes and Engines Division

Mr Keeley is presently employed as a consultant engineer. He graduated from RMIT in 1995 (Aero. Eng) and is studying for a Masters in Aerospace Engineering at RMIT. His past three years of commercial experience include working as a Materials Testing engineer at IPTN Indonesia, and as a Finite Element engineer for the automotive industry. He began working for AMRL in 1994 as a Finite Element engineer and is currently involved in the "Analysis and Validation of Design Procedures for Bonded Repairs"

Contents

Notation

A	Coefficient in equation (10)
B	Coefficient in equation (10)
D	Bending stiffness
E	Young's modulus
E_1	Young's modulus for skin
E_0	Young's modulus for patch
E_C	Transverse tensile modulus for adhesive
E_C^i	Effective transverse tensile modulus of the adhesive
K_I	Mode 1 stress intensity factor
K_{IUP}	Mode 1 stress intensity factor unpatched
K_{IP}	Mode 1 stress intensity factor patched
K_{IC}	Fracture toughness
G_a	Adhesive shear modulus
L	Constant
N	Cycles
a	Half crack length
b	Half panel width
l	Crack tip element size
t_a	Thickness of adhesive
t_1	Thickness of skin
t_0	Thickness of Boron patch
v	Crack opening displacement
w_o	Transverse displacement
λ	Transfer length
σ	Direct stress
σ_o	Direct stress in Boron patch
ν	Poisson's ratio
γ_E	Elastic limit for adhesive shear strain
γ_u	Ultimate failure shear strain for adhesive
τ	Shear stress
τ_e	Elastic limit for adhesive shear stress
τ_E	Equivalent elastic failure stress
τ_p	Ultimate failure for adhesive shear stress
τ_a	Adhesive shear stress
Ω_L	Load attraction factor
Ω_T	Inclusion factor for thermal stresses
χ	Coefficient in equation (10)

1. Introduction

A finite element (F.E.) analysis has been carried out on a RAAF designed boron/epoxy repair to an F-111 in which cracking has occurred. Specifically, the crack was 48 mm, tip to tip, running in a chordwise direction at Forward Auxiliary Spar Station (FASS) 281.28 in the lower skin directly beneath the forward auxiliary spar.

The original design of the repair, ref (1), was according to the RAAF Engineering Standard C5033, ref (2) and is based on equations with closed form solutions. The objective of the current work is to validate the design using an independent approach, in this case the Finite Element (F.E.) method. The repair is also being substantiated through an extensive experimental program, however this report focuses on the F.E. aspects.

The calibration of the baseline F.E. model used in this report has been described in ref (3). Work presented here involves the crack modelling, evaluation and validation of stress intensity factors, and extension of the analysis to model the patch and adhesive. Finally, a comparison will be made between the RAAF Engineering Standard and F.E. results.

Consider now the geometry of the wing. The shaded region in Figure 1 (a) shows the area of the lower port wing skin detailed in Figure 1 (b). Shown in Figure 1 (b) are the fuel flow holes in the forward auxiliary spar together with the crack and patch outline on the outboard location.

The crack in the wing skin runs in a chordwise direction and occurs in a region in which material has been removed from the integral stiffener in the skin to allow fuel to move freely in order to maximise fuel usage. In the design of the wing, side stiffeners have been used in an attempt to restore structural strength.

Inspection areas

(a) Lower surface of port wing

Patch   Crack

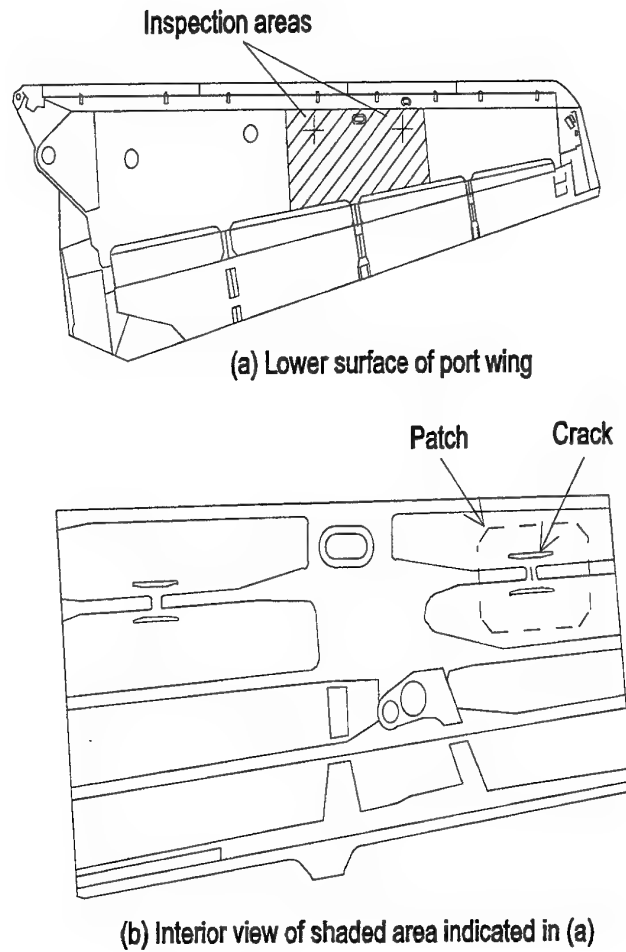(b) Interior view of shaded area indicated in (a)

Figure 1 Geometry of F-111 lower wing skin.

A section view of this area is shown in Figure 2, in which the y axis is in the chordwise direction, the x axis is in the spanwise direction and z axis is in the thickness direction. The crack is shaded and shown in the yz plane.
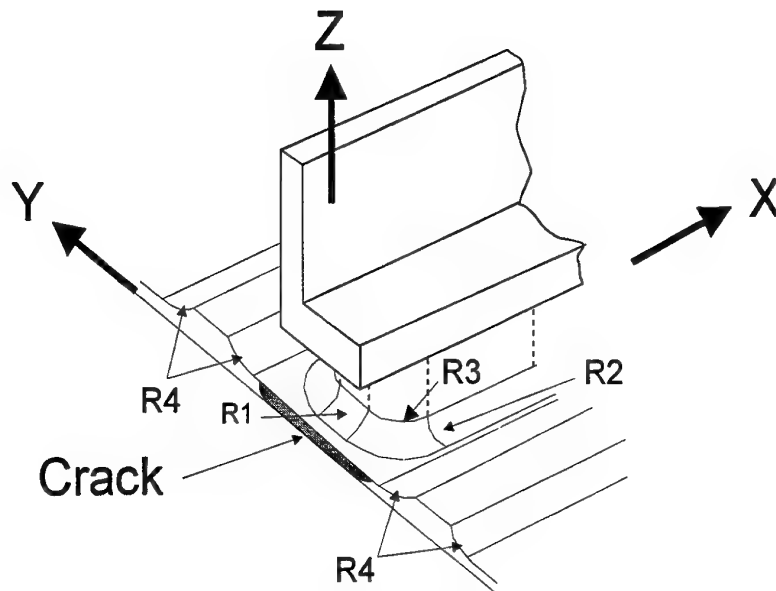
Figure 2 Detail section view of crack and fuel flow hole area.

2. Modelling

2.1 Model description

Firstly, it is necessary to consider the geometry of the region in which the fatigue crack has been found. The crack runs in a chordwise direction and occurs in a region in which material has been removed from the integral stiffener in the skin, as shown in Figure 2. This was to allow fuel to move freely and hence maximise fuel usage. Side stiffeners which can be seen in Figure 1b and Figure 2, were included in the structure in an attempt to restore the structural integrity.

Since the geometry in this area is symmetric about the chordline which contains the crack, it has been possible to use an F.E. 'half model'. This is particularly convenient since it reduces the size of the problem considerably. Given that the size of the patch is 468 mm by 324 mm, the baseline model extends in the chordwise direction from the front spar to the centre spar. In the spanwise direction the model extends beyond the end of the patch to a transverse member, which runs approximately chordwise. The dimensions of the baseline model are shown in Figure 3.
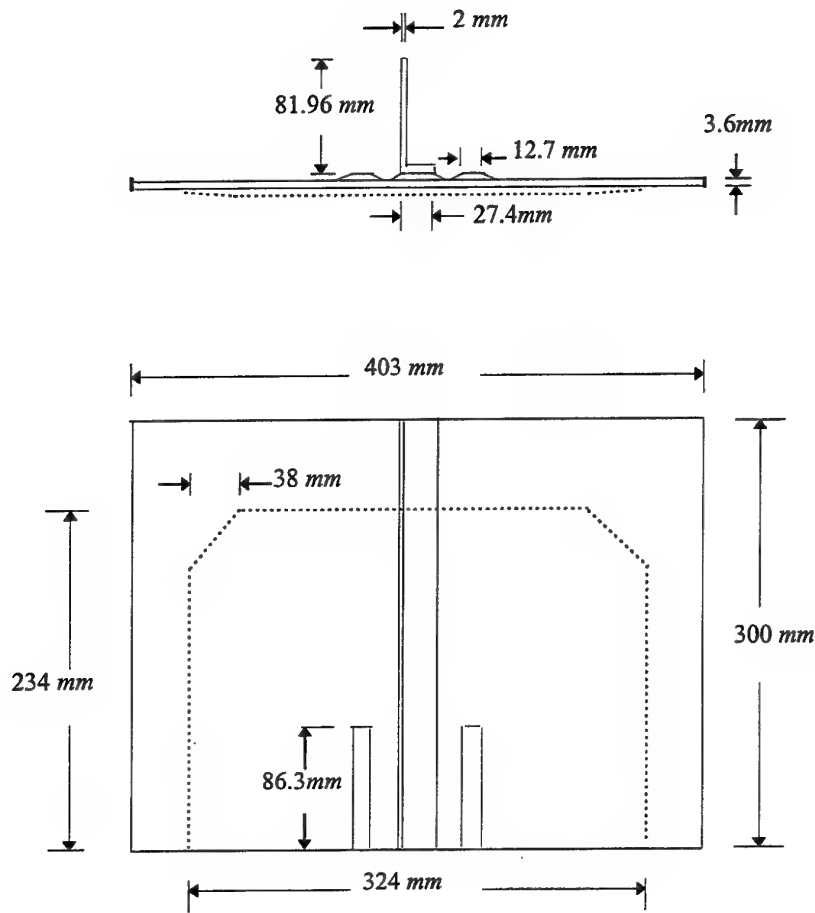
Figure 3 Overall dimensions of baseline F.E. model

As shown in Figure 2, the bottom half of the spar is included in the model, although in this view it has been translated vertically to allow the geometry to be seen in the region of the crack. Note that 4 radii are necessary to define the geometry together with the skin thickness.

For the repair substantiation it has been necessary to base the F.E. models on the engineering drawings and on minimum limits given the tolerances. The minimum skin thickness used is 3.6 mm and the relevant drawings are given in ref (4). It is interesting to note that the skin thickness on a USAF F-111G cracked at the same location was 3.3 mm. The inclusion of the spar in the analysis is important since the spar carries a considerable part of the load, and the spar is connected to the skin by interference fit 'Taper lok' bolts. Modelling of the spar also involves the spar being separated by a very small vertical gap from the skin. This allows connections to be made between nodes on the spar and skin, corresponding to bolt locations. The importance of the inclusion of bolts in the analysis can be seen in deformation pattern shown in Figure 4. Bolt locations have been found to influence the secondary bending in this area. This is

also the location in which fatigue cracking occurred. To prevent 'merging' of the skin into the spar it has been necessary to use gap elements.
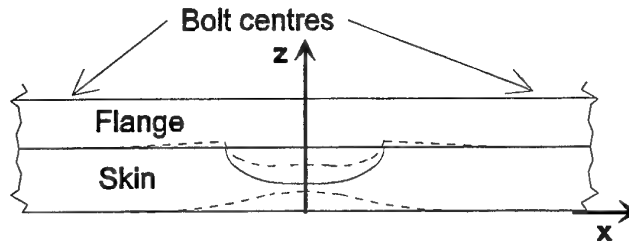
Figure 4   Side elevation of skin & spar flange. Deformation of skin between bolt centres is also illustrated.

Table 1   Material properties of the spar and skin, ref (5).(specification QQ-A-250/4(T851))

Material	E (MPa)	G (MPa)	ν	Yield strength (MPa)	Ultimate tensile strength (MPa)
2024-T851	72397.	27217.	.33	407.	448.

2.2 Assumptions

The following assumptions are made for the geometry and loading of the model.

1.   Loading is in the spanwise direction only, and is taken to be a uniform pressure.

2.   The skin thickness in this model is taken to be uniform, except for the integral stiffeners and spar landing.

3.   The skin material is taken to be isotropic, and whose properties are shown in Table 1.

4.   Simple support conditions have been assumed along the edge of the wing skin which joins the centre and forward spars.

5.   Simple supports are applied to the top of the auxiliary spar web.

6.   Simple support conditions are assumed at the loaded end, which corresponds to a transverse member.

7.   No support conditions are applied to the model in the plane of the crack.

2.3 Geometry

The overall dimensions of the F.E. model are shown in Figure 3. This shows both the plan view of the half model, and the dimensions of the spar. The definition of the radii R1, R2, R3, and R4 are shown in Figure 2. The drawings specify all these radii to be 9.6 mm.

2.4 Elements

In this analysis the use of the prism element which can result in over stiffening of the model, has been minimised. Specifically for the PAFEC program the elements used are:

1.   20 noded bricks
       a)   37110 isotropic, used to model the skin and spar
       b)   37115 orthotropic, used to model the adhesive and boron

2.   16 noded prisms
       a)   37210 isotropic, used for the skin
       b)   37215 orthotropic, used to model the adhesive and boron patch

3.   Gap elements

2.5 Restraints

Figure 5 shows the restraints applied to the model. The directions X, Y, Z have already been defined in Figure 2. Specifically the following restraints are applied:

1.   Skin

       a)   Simply supported in the Z direction applied along the sides corresponding to the front and centre spars.

       b)   Simply supported restraints in the Z direction, applied at the loaded end of the skin corresponding to a transverse member.

       c)   Restraint in the X direction corresponding to the Y-Z plane for which X=0.

       d)   There is one restraint in the Y direction as shown in Figure 5.

2.   Spar

   a)   Simply supported restraints in the Z direction applied along the top of
         the spar web as shown in Figure 5.

   b)   Restraint in X direction corresponding to the Y-Z plane for which X=0.
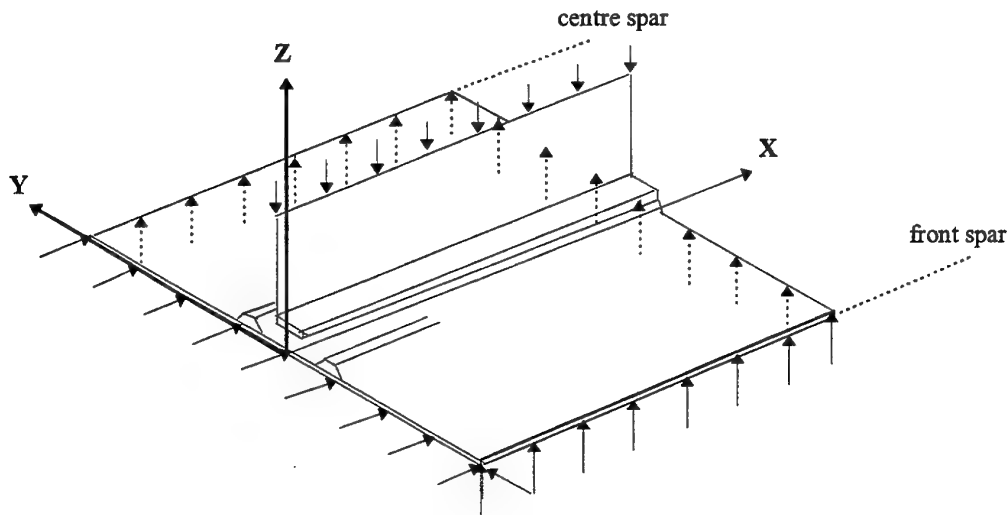
Figure 5. Restraints applied to spar/skin model

2.6 Loading

2.6.1 Flight loads

As stated in section 2.1, it was decided to base the repair substantiation on the
minimum allowable skin thickness of 3.6 mm (this is a conservative approach). Ref (3)
gives the spanwise applied loading (193 MPa) required for the baseline F.E. model to
correctly predict the outside surface strains for a 4.2 mm skin thickness wing under the
Cold Proof Load Test (CPLT) loading. The CPLT loading results in a local bending
moment of 1.60×10^6 inch pounds, whereas the Design Limit Load (DLL) condition at
FASS 281 is 1.82×10^6 inch pounds (see ref (3)). The stress in this location is known to be
a direct function of the applied wing bending moment. The flight load to correspond
to a minimum skin thickness (3.6 mm) wing under DLL was therefore calculated as
follows:

$$\sigma = 193. \, (4.2/3.6). \, (1.82/1.60) = 256 MPa$$

The bolt locations shown in Figure 4 were found to have a strong influence on the
results and were adjusted to a distance slightly closer to the critical region than the

actual location to achieve the best agreement with strain gauge results. A simple explanation is that the clamping effect of the bolt extends a distance outside the bolt diameter.

2.6.2 Thermal loads

The internal stresses and strains in the repair system are affected by the operating temperature in two separate ways as follows:

(a) The mechanical properties of the cured adhesive vary dramatically with operating temperature (see Table 8). At low temperatures the adhesive is much stiffer and the load transfer is therefore significantly different when compared to room temperature. The crack patching efficiency is also significantly affected.

(b) The adhesive bonding the patch to the wing skin is cured at elevated temperature (82°C). The coefficient of thermal expansion of the boron patch material is significantly lower than that for the aluminium wing skin (4.1×10^{-6}/°C versus $23. \times 10^{-6}$/°C). This thermal mismatch therefore results in residual stresses in the system when the operating temperature differs from the bonding temperature. The operating temperature is usually lower than the cure temperature, so residual compression in the boron, tension in the aluminium and shear in the adhesive is expected.

3. Stress and strain distribution

3.1 Strain distribution

The calibration of the baseline F.E. model has been carried out in ref (3). Briefly Figure 6 shows the results of this calibration, where the ε_{xx} strains correspond to the location on the outer surface of the uncracked wing in the critical region. Good agreement has been obtained between experimental data and F.E. results. Secondary bending is shown by the dip in the strain plot, Fig.6.
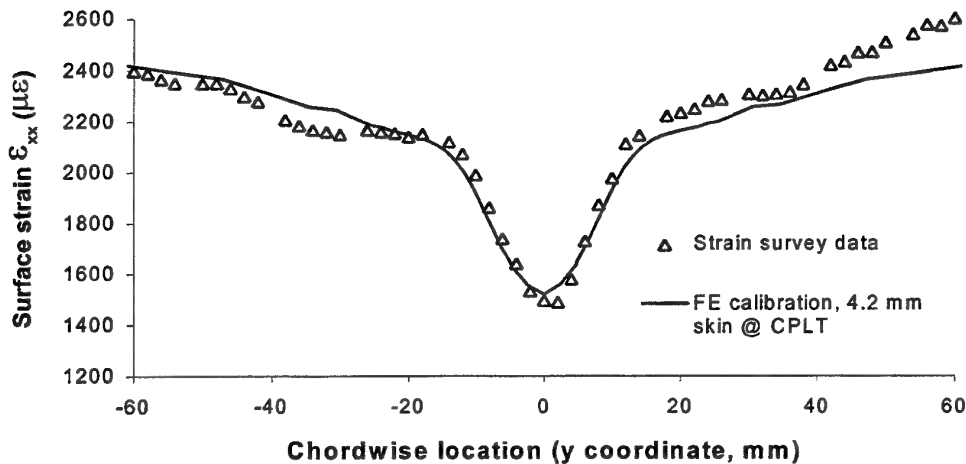
Figure 6 Chordwise variation of strain comparing FE results with strain survey.

The airworthiness aspects require that the repair is effective at Design Ultimate Load (DUL) with wing skins at the minimum thickness tolerances. In this case the minimum skin thickness is 3.6 mm and is less than the calibration model which has a thickness of 4.20 mm. It has been shown that the calibration F.E. model has given good agreement with experimental results, and from this a F.E. model has been developed according to the General Dynamics (G.D.) drawings. Since the only difference between these models is the skin thickness, it was considered that this model is also valid.

Figure 7   Chordwise variation of strain, comparing F.E. results for 3.6 mm skin with calibration F.E. model, at DLL.

The thinner wing skin results in higher stress levels and significantly greater secondary bending. The chordwise ε_x strain variation is shown in Figure 7. Applying the local bending moment and the skin thickness correction factors gives the remote

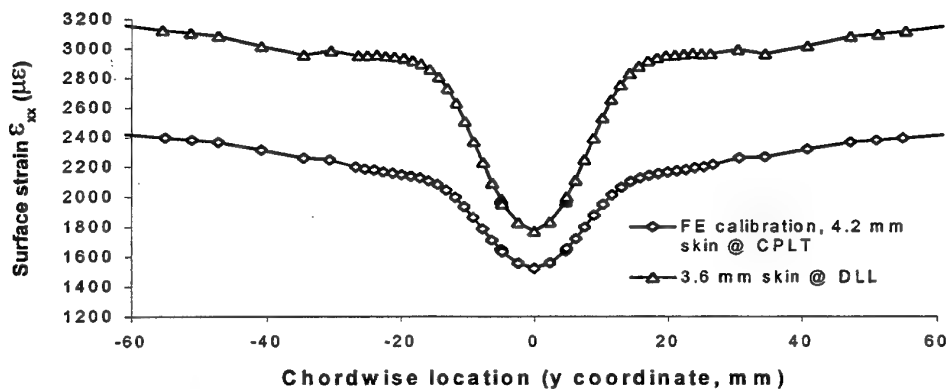stress at Design Limit Load (DLL) as $\sigma^* = 256$ MPa and applies to all figures from this point onwards.

3.2 Stress distribution

From our validated model the stress distribution can be predicted in the area of skin in which cracking occurs. The results in Figure 8 show the chordwise variation of spanwise stress σ_x. (The location y = 0 corresponds to the centreline of the auxiliary spar). On the outside of the skin the stresses are reduced in the vicinity of the spar centreline, but on the inside very high stresses exist and exceed the yield stress in a localised area. (The yield stress for the 2024-T851 is 400 MPa). This explains why cracks develop in this area, starting from the inside and growing through to the outside. Away from this area the stress field is equal to the applied stress of 256 MPa.
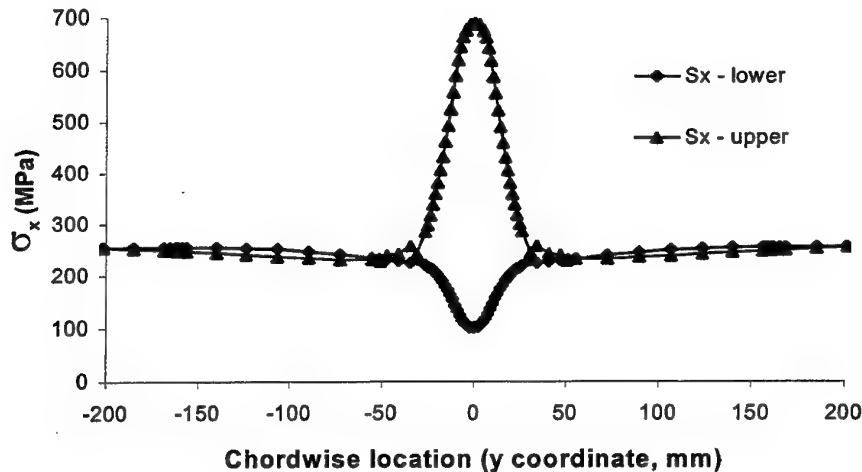
Figure 8 Chordwise variation of σ_x stresses, upper & lower surface of skin, at DLL.

4. Deformation pattern

A significant deformation pattern occurs in the area of cracking. As mentioned previously, bolts have been introduced in to the solution in the area of concern by connecting specific nodes on the skin to the spar. The dotted line in Figure 4 shows the deformation of the skin as a result of secondary bending. Also it indicates that some bending of the lower spar flange will occur. It has been found that the bolt location will have an influence on the secondary bending since it resists the shear between the spar flange and skin. In so doing, it resists the shear deformation and hence bending in that area. In fact, the calibration of the model in ref (3) involved the adjustment of the

bolt locations to get the best results. Clearly, the use of gap elements is fundamental in obtaining the correct solution. In this respect the solution is non-linear since the first solution must define the deformation, and subsequent iterations must produce a compatible solution in which the skin does not 'merge' into the spar.

The other area of concern is at the end of the patch, where the patch picks up the load from the skin. Some bending and shear will occur in this area.

5. Cracked and unpatched model

5.1 Description

Firstly, the length of the crack found in aircraft A8-145 was 48 mm tip to tip on the inside of the wing, while the length of the crack on the outside of the wing skin was considerably shorter (of the order of 6 mm). Similar cracking has occurred to a USAF F-111G in the same area and a fractographic analysis has shown that the crack had started as an elliptical crack and eventually grew through the outer surface of the wing skin. In the analysis presented here the crack will be modelled as a through crack. Firstly this is more convenient, and secondly the crack in the USAF F-111G was almost through to the outside surface, hence this assumption is only slightly conservative.

The crack is most conveniently included in the model firstly by not applying restraints in the x direction for those nodes lying in the plane of the crack. Secondly, the elements surrounding the crack tip are prism elements with the midpoints shifted to quarter points to achieve the $1/r$ stress singularity.

5.2 Stress intensity factor results

The crack opening displacement method (COD) is used to calculate the mode 1 stress intensity factor K_I. This is given by ref (7) for plane strain as:

$$K_I = (EV/(4.(1-v^2)))\sqrt{2\pi/(L(1-(L/(2a))))} \qquad ...(3)$$

and for plane stress as:

$$K_I = (EV/4.)\sqrt{2\pi/(L(1-(L/(2a))))} \qquad ...(4)$$

where E = Young's modulus
  v = Poisson's ratio
  V = displacement
  L = length of the element as shown in Figure 9.
  2a = crack length (tip to tip).

In terms of fracture toughness, the thickness of the skin material corresponds to the transition region of plane stress to plane strain. As a result, the use of the plane stress,

equation (3), is conservative because it gives a higher value of K_I. Also for best results $l/a < 1/20$, however it is known that very small values of l/a may underestimate K_I.

The validation of this formula has been carried out using a 3D centre cracked panel of thickness of 3.6 mm, which is shown in Figure 9. A closed form solution is available, ref (8), and for plane stress is given by:

$$K_I = \sigma\sqrt{\pi a}\left(1 + .128(a/b) - .288(a/b)^2 + 1.523(a/b)^3\right) \qquad ...(5)$$

where 2b = the width of the panel
 2a = the crack length tip to tip

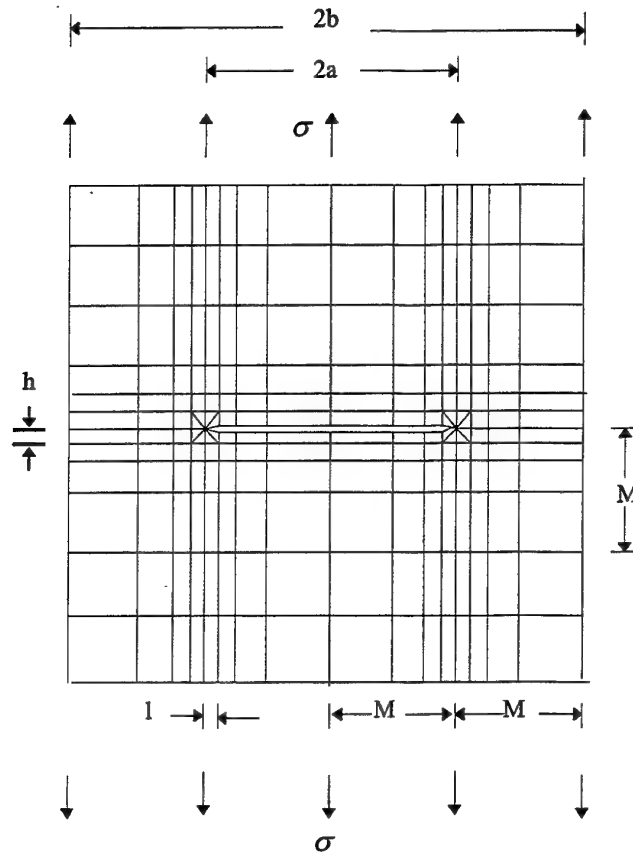This formulae is applicable in the range $0 < a/b < 0.7$

Figure 9. Mesh for centre cracked panel.

The F.E. results for a range of mesh ratio's denoted as 'M', in Figure 9. are given in Table2. This ratio is simply a means of generating a gradation of elements. A comparison of the results has shown that the error of 1.4% has been achieved with a

12

fine mesh, while a relatively coarse mesh has achieved 6% error. The error is based on equation (5) being correct. Also, the size of the crack tip element 'l' results in significant error for values of $l/a < 0.005$. The height of the crack tip is defined as 'h' as shown in Figure 9., and the h/l ratio is also shown in Table 2. While meshing requirements for the F-111 wing F.E. model have restricted the size of the crack tip element, the value of l is 0.3 mm, and for the 48 mm crack the l/a ratio is 0.0125. As a result, an error of less than 5% is expected. The dimensions 2a and 2b are 500 mm and 1000 mm respectively, with a thickness of 10 mm.

Table 2 Validation of COD method for determination of K_I

Mesh ratio	h/l	l/a	K_I (plane stress) $(MPa\sqrt{m})$	% error
1 2 3	0.5	0.02	1.109	-6.2
1 2 3 4	0.5	0.02	1.141	-3.5
1 2 3 4 5	0.5	0.02	1.186	-2.2
1 2 3 4 5 6	0.5	0.02	1.163	-1.6
1 2 3 4 5 6 7	0.5	0.02	1.165	-1.4
1 2 3 4 5 6 7 8	0.5	0.02	1.166	-1.4
1 2 3 4 5 6 7 8 9	0.5	0.02	1.165	-1.4
1 2 3 4	1.0	0.01	1.115	-3.5
1 2 3 4	1.0	0.005	1.052	-11.1

The stress intensity formula was therefore considered valid, and the crack elements were introduced into the wing skin model.

Stress intensities have been evaluated at three points through the wing skin thickness. These correspond to inner, middle and outside surface of the skin. These values vary slightly, and reflect the bending taking place, however only an average value is considered. Also, the result from each crack tip varies slightly, and in this case it is necessary to calculate the root mean square stress intensity factor. Figure 24 shows the variation of stress intensity with crack length for a number of configurations. At present only the cracked and unpatched case (skin only and skin/spar) will be considered. Each stress intensity curve contains 8 data points and the cracks range in length from 15 - 80 mm, measured tip to tip.

Before the spar/skin model was adopted a skin only model was considered. However it was clear that the spar, which bridges the crack, would provide more restraint to crack opening as the crack increased in size. This effect is clearly seen in Fig. 24 in which the spar reduces the stress intensity by 20% for large crack lengths. As expected, for small cracks, the spar has less influence.

The value of the stress intensity factor is dependent on the 3D geometry and crack length. In the region of the central stiffener the skin/spar model gives values of $50 MPa\sqrt{m}$ for crack lengths of 15 mm. As the crack grows the stress intensity increases to $60 MPa\sqrt{m}$ at the edge of the central stiffener. Beyond this point the stress intensity does not change, presumably as a result of the crack tip moving away from

the area of high stress. In between the central stiffener and the auxiliary stiffener the stress intensity rises, however it decreases to $50MPa\sqrt{m}$ as it enters the auxiliary stiffener. Once the crack tip reaches the flat top surface of the stiffener the stress intensity increases again. Although cracks above 80 mm have not been considered, it is expected that the stress intensity will rise rapidly as the crack grows outside the auxiliary stiffener.

The value of fracture toughness given by ref (1) is $46MPa\sqrt{m}$, hence without a repair scheme failure would be predicted to occur at 77% of Design Limit Load (DLL).

6. Patched model

6.1 Description

The orientation of the plies used for the repair scheme is shown in Figure 10. and has been obtained from ref (1). The patch consists of 14 layers of Boron with a lay-up of $\left[0_2,\pm45,0_3\right]_s$. The order of the lay-up is given in Table 3 where layer 1 is the first and layer 14 is the last. The patch has an overall spanwise dimension of 468 mm and a chordwise dimension of 324 mm. Also the patch is rectangular but with cut-off corners.

Layer 1, 14
Layer 2, 13
Layer 3, 12
Layer 4, 11
Layer 5, 10
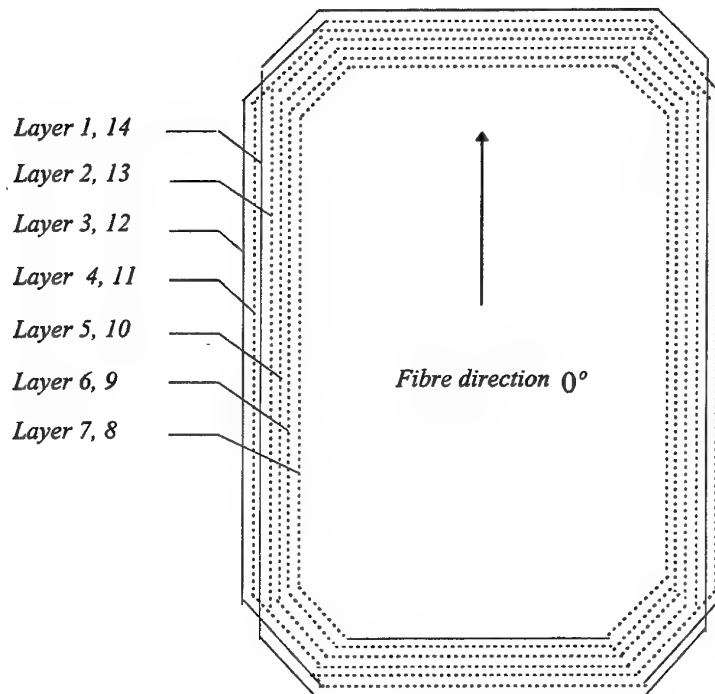Layer 6, 9
Layer 7, 8

Fibre direction $0°$

Figure 10 Lay-up configuration for boron patch.

In the F.E. analysis the use of symmetry has allowed the use of a half model as shown in Figure 11. However, the model still consists of 2,000 20 noded brick elements and 16,000 nodes. As a result of computer size limitations and numerical accuracy, there is no one model which is used to predict all results. It has been necessary to create a number of models, each with a specific area of refinement. This has allowed a detailed investigation into areas in which stress concentrations exist.

Table 3 Ply lay-up order

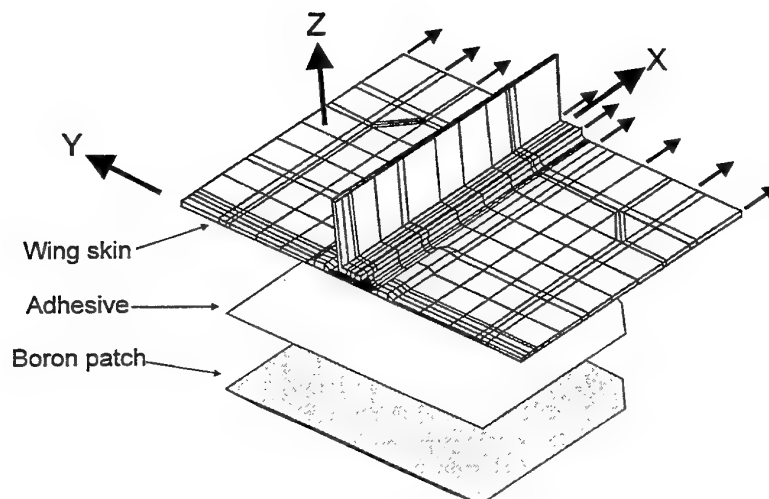| Layer	Ply angle (deg)
1	0
2	0
3	45
4	-45
5	0
6	0
7	0
8	0
9	0
10	0
11	-45
12	45
13	0
14	0

Figure 11. Spar/skin F.E. model with outline of adhesive and boron patch.

6.2 Patch details

In the F.E. analysis the Boron patch is modelled as a homogenous orthotropic material in which the material constants are obtained using laminate theory. The properties of the unidirectional Boron are shown in Table 4 and 5 while the overall properties of the laminate are shown in Table 6, and do not vary significantly over the operating temperature of the aircraft. However compression strength properties do vary significantly over this temperature range. The material compliances for Boron/epoxy laminate used in the model are shown in Table 7. The F.E. outline of the patch is slightly simplified as shown in Figure 11. However the F.E. idealisation does include the patch taper in all directions. As previously mentioned, a 'half' model is used and is shown in Figure 11 as an exploded view, including the adhesive.

Table 4 Mechanical properties for 5521 boron/epoxy, ref (9)

Material property	Room temperature	121° C
Tensile strength (MPa)	1520	1450
Tensile modulus (GPa)	210	210
Compressive strength (MPa)	2930	1250
Compressive modulus (GPa)	210	210
Flexural strength (MPa)	1790	1720
Flexural modulus (GPa)	190	17
Interlaminar shear (MPa)	97	55
Coeff. thermal exp /° C	4.5	4.5
Density g/cm³	2.0	2.0

Table 5 Properties for a single layer of Boron, ref (10)

E_{11} =207000. MPa	E_{22} =19000. MPa	G_{12} =4800. MPa	v_{12} =.21	$\alpha = 4.1x10^{-6}\,/^{0}\,C$

Table 6 Overall properties of the Boron patch for patch lay-up of $\left[0_2,\pm45,0_3\right]_s$

E_{XX}=156107.	E_{YY}=29781.	v_{XY} =.574884	v_{YX}=.109675	G_{XY}=190651.

Table 7 Compliances for Boron/epoxy laminate input to PAFEC.

S_{XX} =.640588x10^{-5} (=1/E_{XX})	S_{XY}=.368264x10^{-5} (=$-v_{XY}/E_{XX}$)	SH_{XY}=.524519x10^{4} (=1/G_{XY})
S_{YY}=.335779x10^{-4} (=1/E_{YY})	S_{YZ}=.705135x10^{-5} (=$-v_{XY}/E_{YY}$)	SH_{YZ}=.208333x10^{-3} (=1/G_{12})
S_{ZZ} =.526087x10^{-4} (=1/E_{ZZ})	S_{ZX}=.134524x10^{-5} (=$-v_{XY}/E_{XX}$)	SH_{ZX}=.208333x10^{-3} (=1/G_{12})

6.3 Adhesive details

The properties of the FM73 adhesive are temperature dependent and are given in Table 8 for 3 different temperatures as required for the substantiation of the repair. In this repair the adhesive consisted of 2 films with a total thickness of 0.254 mm after the repair application.

6.4 Modelling of Thermal Effects

Stresses and strains in the various elements of the repair are significantly influenced by temperature. This is for two reasons:

(a) The properties of the adhesive change significantly with temperature.

(b) The differences in thermal coefficient of expansion for the aluminium compared with the boron laminate results in a thermal "mis-match" which leads to residual stresses and strains.

The thermal mis-match residual stresses can be either beneficial or detrimental, depending on the location and sign of the mis-match. If the coefficient of thermal expansion of the aluminium wing structure is greater than that of the boron laminate, then at the end of the patch the thermal residual adhesive shear stresses are opposite in sign to the adhesive shear stresses that arise as a result of flight loads, and are beneficial. Over the crack region however, the residual thermal adhesive shear stresses are the same sign as the shear stresses due to flight loads, and are detrimental. If however, the thermal coefficient of thermal expansion of the aluminium wing structure is less than that for the boron laminate then the reverse of that just stated, is true.

For the analysis presented in this report the adhesive properties relevant to the temperature for the case being examined are always used. The thermal mis-match is a significantly more complex analysis and it is only included where appropriate. The results detailed in section 7 indicate where the thermal mis-match effects have been included and why.
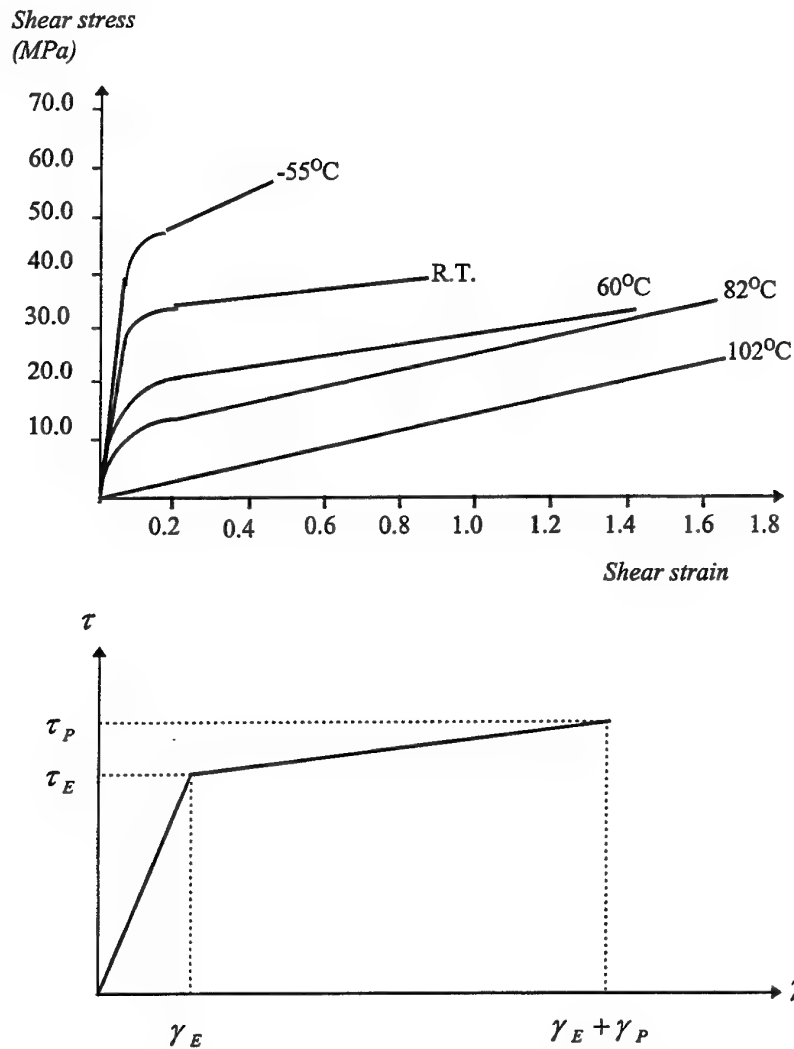
Fig 12a. Stress vs strain curves for FM73, top; and idealised curve, bottom.

The stress-strain curves for FM73 adhesive are shown in Figure 12 and are taken from the manufactures data ref (11). At the lower temperatures the shear modulus and strength is higher compared to that at high temperatures. However, at lower temperatures the strain to failure is lower than that at high temperatures. The failure of an adhesive is governed by the strain energy under the stress strain curve taken to failure. It is well known that the adhesive transfers load primarily by shear. Also, the relatively low adhesive yield stress results in a considerable amount of plasticity. However for convenience, the F.E. analysis will be restricted to a linear elastic analysis. It is possible to carry out a strength analysis using a linear elastic analysis in which an equivalent elastic stress (or strain) is used to predict failure. In this case the stress (or strain) must be based on the strain energy under the stress strain curve taken to failure.

The elastic behaviour of an adhesive in a bonded joint usually involves a peak shear stress at the start of the joint, then an exponential decay. This is the solution predicted by the 1D differential equation, ref (12). The F.E. analysis however, shows a rapid rise to a peak shear stress at a distance approximately equal to the adhesive thickness. In the analysis presented here we will examine the adhesive stress state at a number of critical points in the patch. Critical points in the adhesive have been identified using graphical means.

Table 8 Variation of FM73 adhesive properties with temperature.

Temperature	E (MPa)	G (MPa)	ν
$-40^o C$	2408.	892.	.35
$-32^o C$	2392.	886.	.35
RT	2273.	842	.35
$75^o C$	875.	324.	.35

7. Results

7.1 Patched uncracked

The aim in this section is to identify any detrimental effects that may result from the patching of a structure which is uncracked or contains a very small crack. Also it is useful to assess the ability of the patch in being able to stop the initiation of a crack. The internal stresses and strains due to the thermal mis-match are not evaluated for the patched uncracked model. The reason is because the prime area of concern is the shear and peel stresses in the adhesive at the end of the patch, and the sign of these is usually opposite to the stresses which result from the applied flight loads, i.e. the residual shear stress at the end of the patch is relieved by the applied flight loads. In terms of the boron strains, it was useful to compare the F.E. strains with measured strains from the actual wing under load. The measured strains were taken from a zero set for the cured patch in place, i.e. the residual strain was not included.

7.1.1 Boron strains

After the repair to A8-145, a strain survey was carried out by the RAAF, ref (13), in which three gauges were attached to the outer surface of the boron patch to measure spanwise strains. The aircraft was loaded on the ground by applying loads to hard points on the wing. One gauge was located directly over the crack region on the spar centre line, while the remaining gauges were located in the same chordwise plane but offset 124*mm* either side of the spar centre line. To make valid comparisons with the flat skin F.E. model, the offset gauge results have been averaged. The results have been factored up to the strain expected at DLL and are shown on Figure 13 together with F.E. predicted results. The centre gauge gives lower results than the F.E. predictions, however the averaged results for the offset gauges, which are in a low spanwise strain

gradient, agree to within 10%. There is however, some uncertainty about the comparison using these strain gauge results, since the wing skin thickness of aircraft A8-145 is unknown

Early F.E. models predicted strain levels of approximately 7000 microstrain on the upper surface of the boron/epoxy laminate. However the use of two or more elements through the thickness of the boron laminate have reduced these strains to levels of 2700 microstrain as shown in Figure 14 and 15. It is however, not possible to continue this level of refinement to the end of the patch. As a result the models with one element through the thickness of the boron laminate are still used to predict boron and adhesives stresses where the patch tapers to one layer.

Another aspect of the uncracked case is that the boron/epoxy patch picks up load even though a crack does not exist. The strain level at a distance 60 mm away from the crack is approximately 2200 microstrain on the lower surface, and it will be shown later that this does not change even after a crack is introduced.
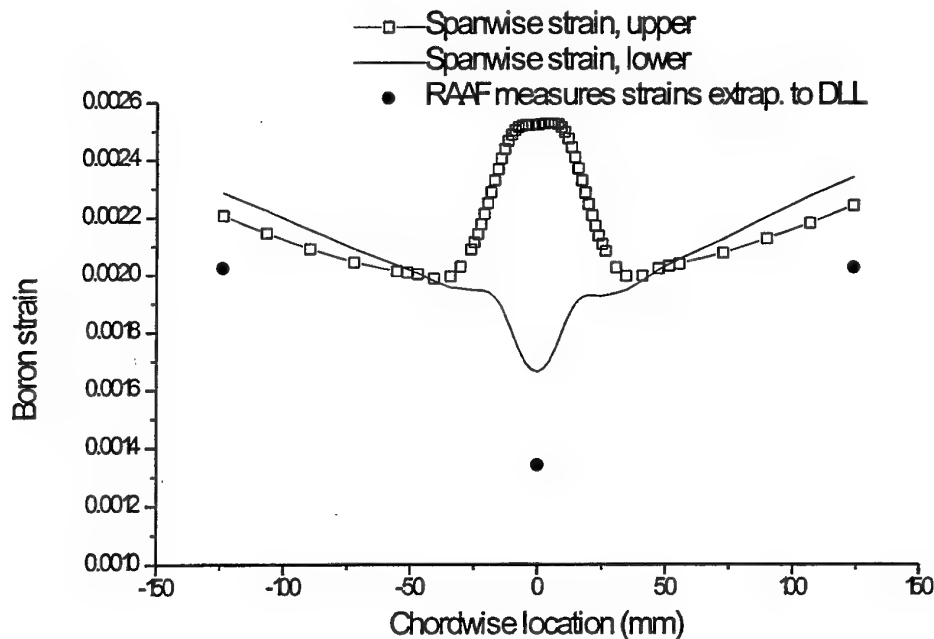
Figure 13. Chordwise variation of Boron strain at the crack location ,room temperature case, uncracked case.
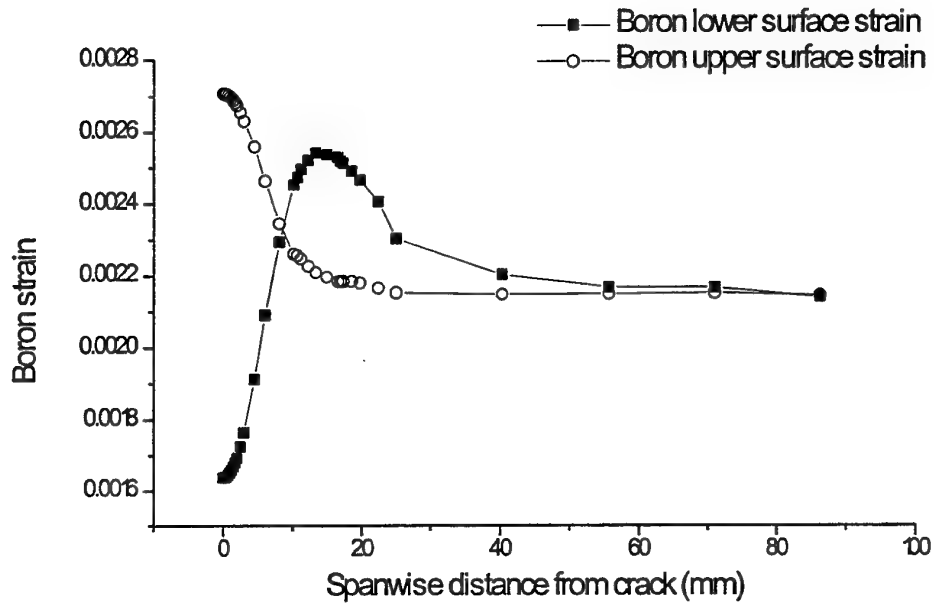
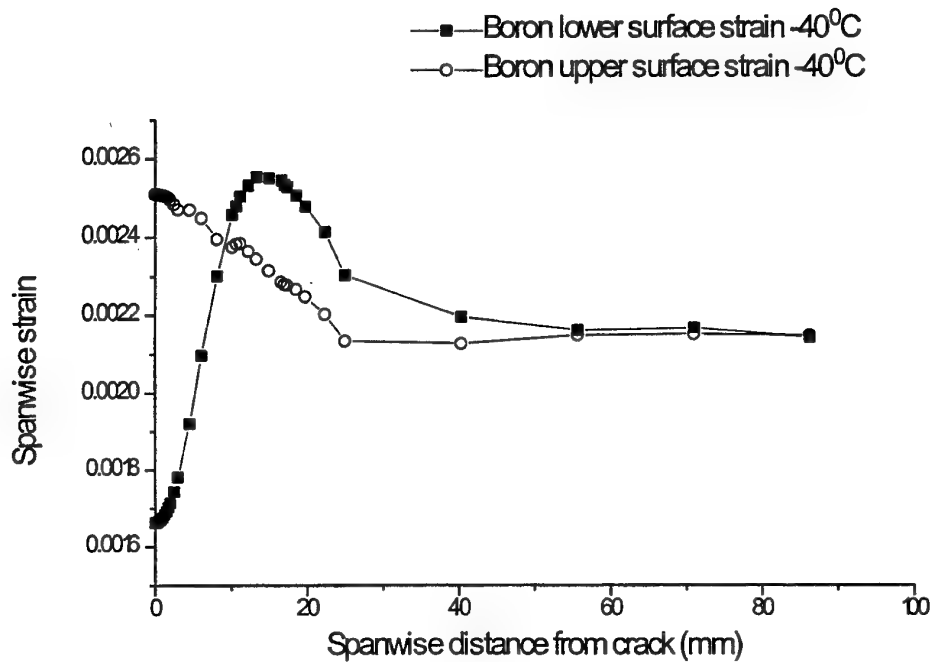*Figure 14. Boron strains, +75⁰C, for the uncracked case.*

Figure 15. Spanwise variation of boron strains, -40⁰C for the uncracked case.

7.1.2 Adhesive stresses

7.1.2.1 Temperature of -40°C

Adhesive τ_{zx} shear stresses are shown in Figure 16 and correspond to the end region of the patch. Figure 16 shows the state of stress at four different stations. The first being exactly at the end of the patch, while the next is 0.10 mm from the end and so on. The adhesive starts at a low value and reaches a maximum value at approximately 0.29 mm from the end of the patch. Each curve has the same characteristic curve with two peaks which correspond to the chamfered corners of the patch. Also the stress value corresponding to the location of the forward auxiliary spar (chordwise co-ordinate = 0) is considerably lower than the peak values. It appears that the bending of the unsupported plate away from the spars, is also increasing the shear stress.

The Von Mises stress distribution is shown in Figure 18, and has the same characteristics as the shear stress distribution. The Von Mises stress distribution is more representative of the failure stress for the adhesive since it also considers the contribution of other stress components.

The peel stress distribution is shown in Figure 17 and is a smoother distribution than that given in Figure 16 and 18. However, the peel stress is still higher where the plate is unsupported, and clearly the bending of the plate is responsible for this behaviour.

Margins of safety will not be given here, however in the later sections the results corresponding to cracks, show maximum stress values equal to those obtained in a patched uncracked structure.

7.1.2.2 Temperature of +75°C

The characteristic curves obtained for results of -40°C are also obtained at +75°C and are shown in Figures 19, 20 and 21. The only difference being the lower magnitude of the stresses. It will shown later, that when a crack is introduced, the adhesive stresses at the end of the patch remain the same.
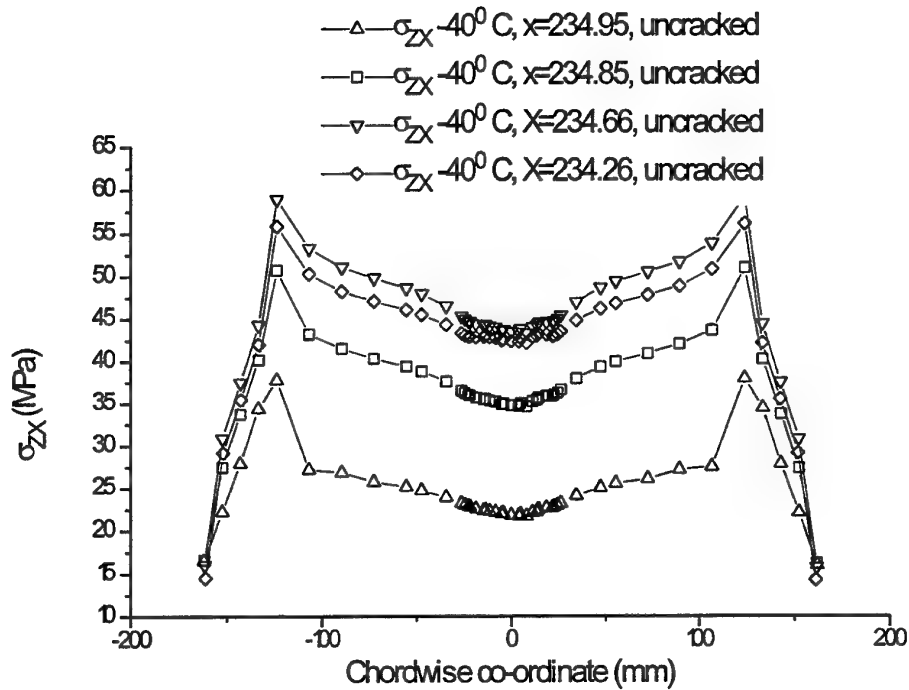
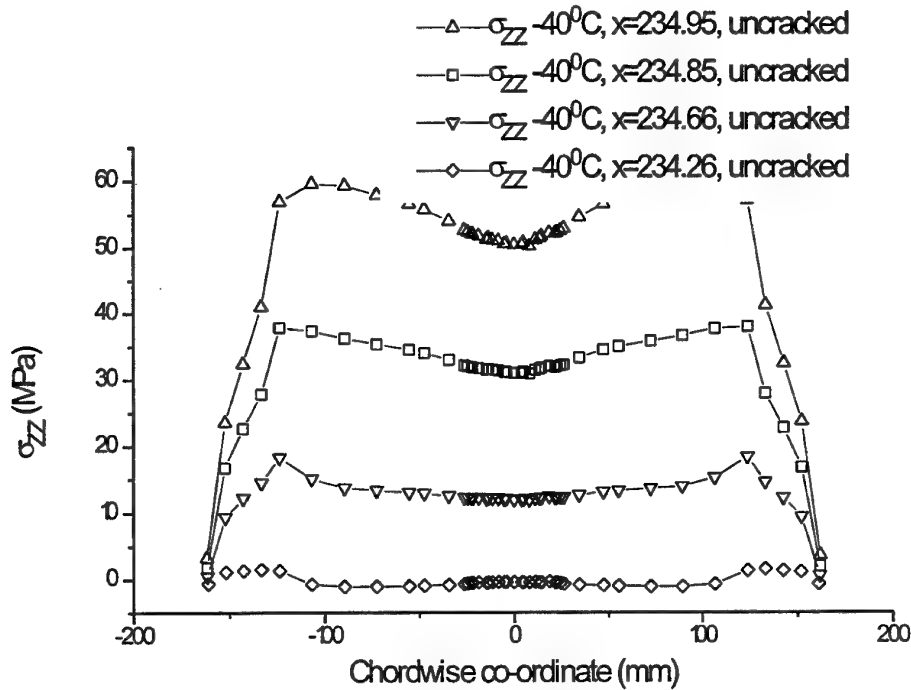*Figure 16 Shear stresses at end of patch for -40° C case.*

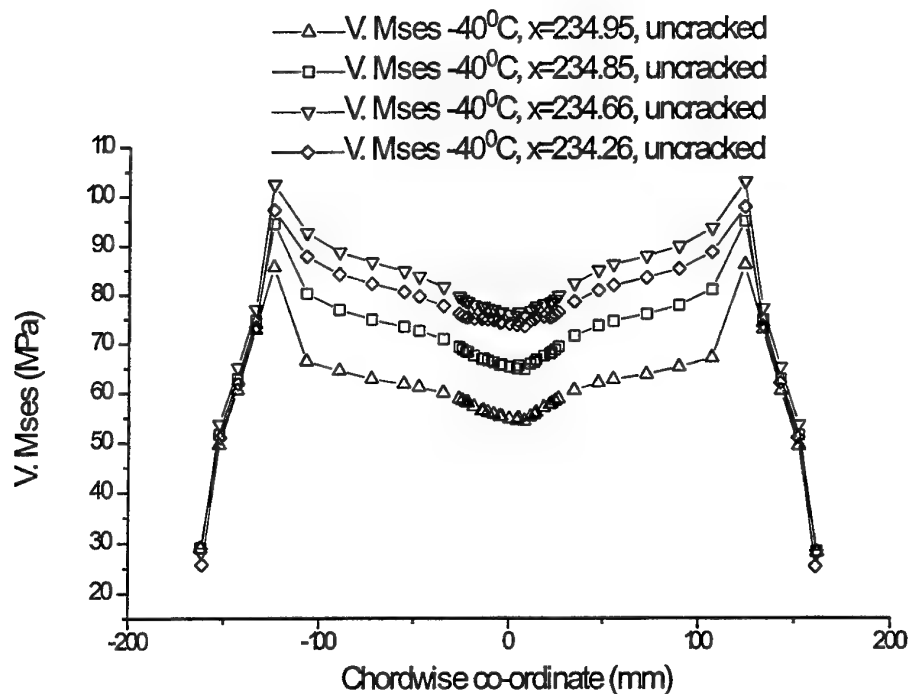*Figure 17 Peel stresses at end of patch, -40°C.*

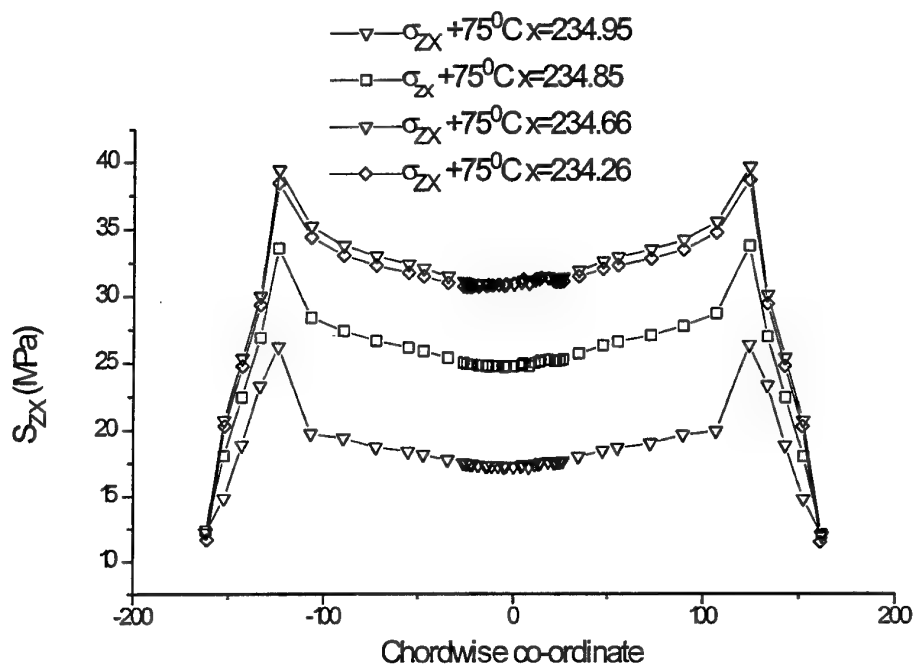*Figure 18 Von Mises stresses at end of patch, -40ºC.*

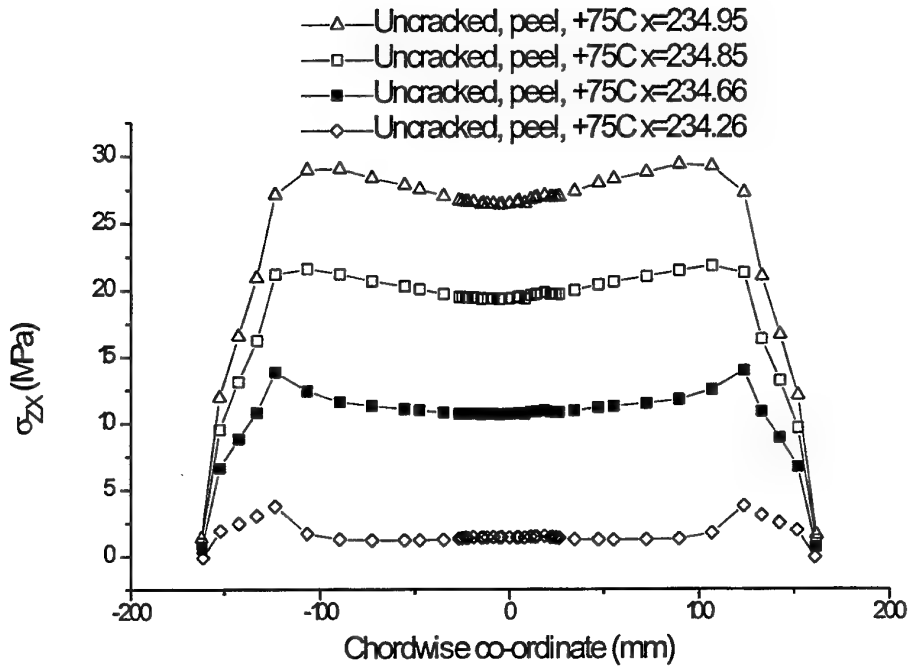*Figure 19 Shear stresses at end of patch, +75ºC.*

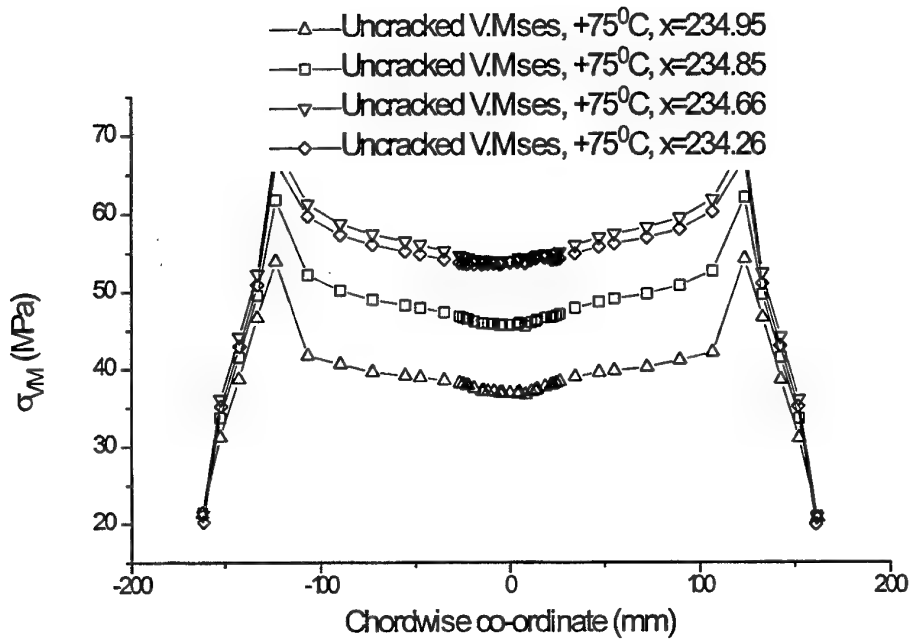*Figure 20. Peel stresses at end of patch, +75⁰C .*

Figure 21 Von Mises stresses at end of patch, +75⁰C.
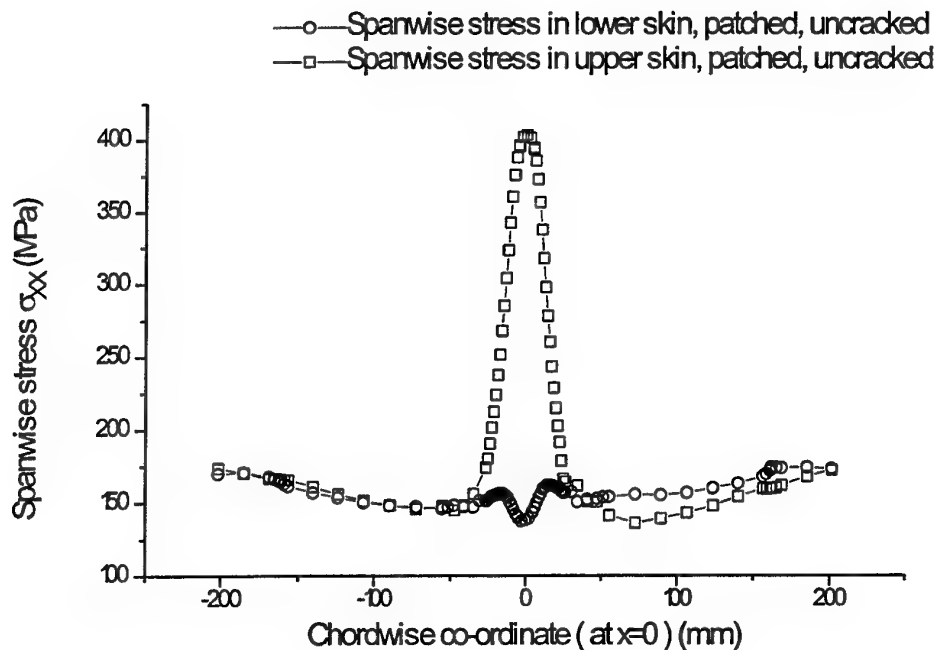
Figure 22   Spanwise stresses in the skin for the uncracked and patched case, DLL, room temperature.

7.1.3 Stress distribution in the skin

The results in Figure 22 show that the stresses in the critical area have been reduced to approximately 400 MPa, which is the yield stress for 2024-T851. This stress is significantly less than the value give in Figure 8 for the unpatched, uncracked case, and there may be a case for patching all aircraft in the fleet. Also in comparison to Figure 8, the background stress level (approximately 160 MPa) under the patch is significantly lower than the applied stress of 256 MPa. Using graphical means, it has been determined that no significant detrimental skin stresses have been found beyond the end of the patch.

7.2 Patched and cracked

In this section we will consider the effectiveness of the patch and stress intensity factors for a range of crack lengths. Also the adhesive and Boron stresses will be considered for the 48 mm crack length. The stress intensity factor work does not (except where indicated) take into account the thermal mis-match effect, but does account for the adhesive properties at the specified temperature. A validation of the thermal stress capability of PAFEC will now be carried out.

7.2.1 Validation of thermal stress analysis

Experimental data has been used to validate the thermal stress capability of the PAFEC F.E. program. In ref (14), an aluminium plate 115 mm x 25 mm x 1.56 mm has been reinforced either side with 3 layers of a unidirectional Carbon fibre and cured at 126°C using AS126 adhesive. Use of Carbon fibre has allowed measurement of direct residual stress using X-rays. A F.E. analysis has been carried out for this structure whose material properties are shown in Table1. The results are shown in Figure 23. Approximately 6% error occurs between the F.E. and experimental values for direct stress at the midspan of the plate. The source of the error is not known. From this data the residual shear stresses can be inferred. Note the agreement of direct stresses at the end of the patch is important, since this largely determines the shear stress distribution. The experimental data points show some scatter in the area in which the direct stress is rapidly changing. The plot shown in ref (14) does give the 95% confidence limit and the F.E. results correspond closely to this plot. Some of the experimental data on the plot corresponds to the other end of the structure, however it is more convenient to include this data as shown in Figure 23. The comparison with the F.E. model and experimental data gives confidence for the prediction of residual stress in the lower skin repair.
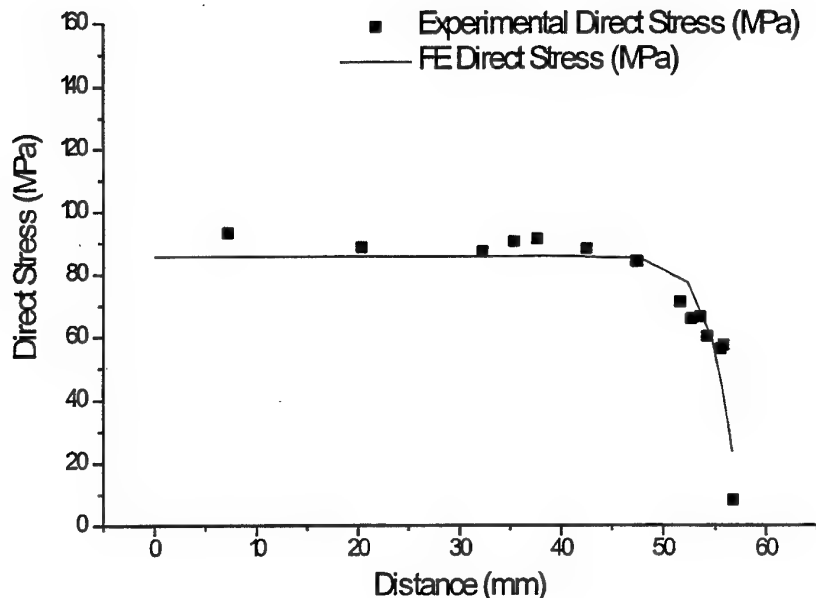

Fig 23. Comparison of Experimental residual data and F.E. results.

Table 9 Material properties corresponding to the thermal residual stress experiment, ref (14).

Carbon fibre	7075-T6	Adhesive
E_1=130000. MPa	E_T =71016 MPa	G_a=700. MPa
G=7000. MPa	E_C =72397 MPa	V =0.35
E_1/E_2=15.4	V =.3	t=.15
V =.3		
α_1 =0.5x10^{-6}	α =23x10^{-6}	0.

7.2.2 Stress intensity factors

Although the crack length, 2a, measured tip to tip, for the repaired aircraft was 48 mm, a study of crack lengths varying from 15 - 80 mm was considered. At an early stage in the project skin models were considered and constrained to simulate the effect of the spar. Results shown in Figure 24 show that the skin models predicted high stress intensity values, K_I. The effect of the spar is substantial in reducing the value of K_I, particularly for large crack lengths. From Figure 24, it is evident that the RAAF designed patch is very effective in reducing the stress intensity factor by almost 50%. Using a crack growth law, the reduction in crack growth is:

$$(\delta a/\delta N)_c/(\delta a/\delta N)_{uc} = (K_I/K_{Ip})^n \qquad \qquad ...(1)$$

where for aluminium alloys n varies from 3 to 4. Using a value of n = 4 gives a reduction of crack growth by a factor of 50. Experimental results to date have shown a reduction in growth by a factor of 100, however the differences in the results may be due to other experimental factors. The dotted horizontal lines shown in Figure 24 corresponds to the value of K_I predicted by C5033, ref (1), for temperatures of -40°C and +75°C, and includes the contribution of thermal stresses. Note the F.E. results shown in Figure 23 do not include thermal residual stress.
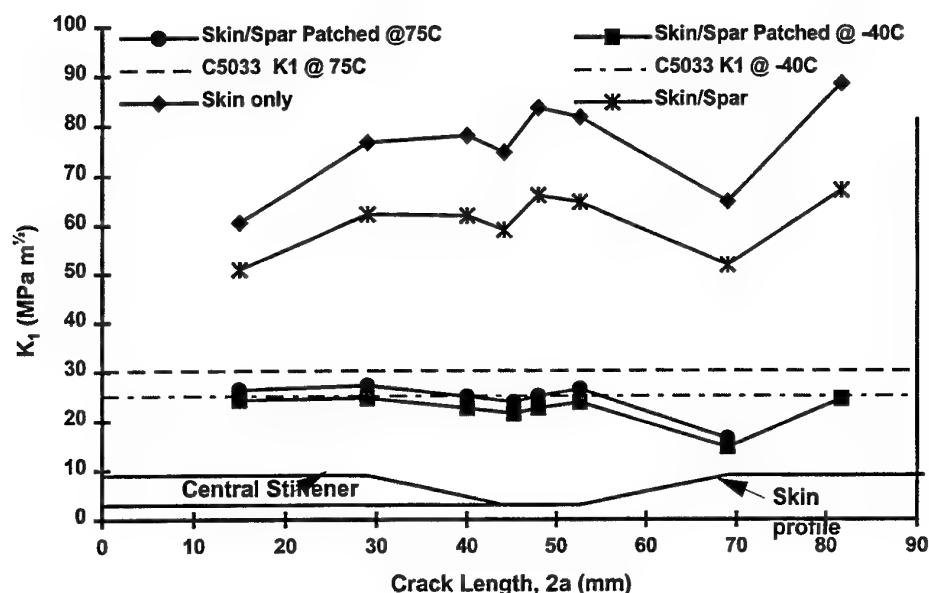
Figure 24 Stress Intensity factor versus crack length, at DLL.

The F.E. model was run including the thermal effects for a crack length of 48 mm only. This was done for a range of possible coefficients of thermal expansion for the skin material and the results are shown in Table 10. This was done at -40°C because this condition gives the greatest temperature difference for the cure condition at 82°C. At an operating temperature of 75°C the residual thermal stresses are negligible. From Figure 24, at the 48 mm crack length and the -40°C condition, the F.E. without thermal effects gives a K_I of approximately $23.0 MPa\sqrt{m}$. This compares with a result from Table 10 with $\alpha = 15.3x10^{-6} /^0 C$ (as used in C5033) of $26.7 MPa\sqrt{m}$. The C5033 prediction is $25.1 MPa\sqrt{m}$. Including the thermal effect therefore increases the K_I prediction by about 16 percent. The C5033 prediction is considered to be in good agreement with the F.E. result.

The result in Table 10 corresponding to $\alpha = 23. x10^{-6} /^0 C$ is given and represents the case in which the material value of the coefficient of thermal expansion of the skin is used, and over predicts the value of K_I. The F.E result from Table 10 for $\alpha = 6.0x10^{-6} /^0 C$ was included because this is the result which has been derived from strain gauge measurements, ref (15), on a full scale F-111 wing. The extreme values for these strains are shown in Table 11. This indicates that the value of α assumed by C5033 is very conservative, and the residual thermal stresses experienced in the repair are probably much lower than previously thought.

Table 10. F.E. stress intensity values at -40⁰C, corresponding to different coefficients of thermal expansion.

α (/⁰C)	23.x10⁻⁶	15.3x10⁻⁶(C5033)	6.0.x10⁻⁶ (Ref (15))
$K_I \left(MPa\sqrt{m} \right)$	31.20	26.68	22.69

Table 11 Strain gauge readings corresponding to a simulated bonding process.

Spanwise strain near front spar	Spanwise strain near middle spar
-100. µε	-370. µε

7.2.3 Adhesive stresses

The adhesive used is FM73 which is cured at a temperature of 82°C and whose properties are temperature dependent. For airworthiness requirements, a range of temperatures must be considered for the design calculations: -40, -32 and 75°C. The F.E. analysis also includes the contribution due to thermal stress. In the region adjacent to the crack, the thermal residual shear stress in the adhesive is of the same sign as the stress due to the flight loads so the two are added. In the region at the end of the patch, the reverse is true because the residual stress relieves the flight load. A conservative approach is taken in this report; the residual thermal effects are included in the F.E. analysis in the region of the crack, and are ignored at the end of the patch. The results are derived from different runs of the same F.E. model.

7.2.3.1 Adhesive shear stresses

Firstly consider the τ_{zx} shear stresses over the crack region as evaluated by the 3D F.E. analysis in the mid plane of the adhesive, shown in Figure 25, for the case of -40°C. The boundary condition at the crack requires that $\tau_{zx} = 0$ at $x = 0$.
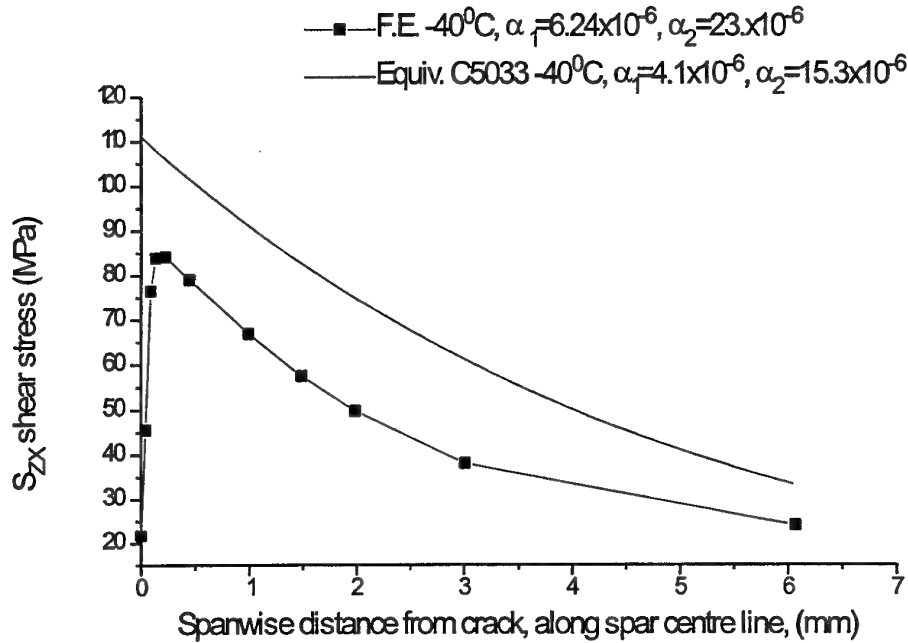
Figure 25 Adhesive shear stress (τ_{zx}) near crack, -40°C, at DLL.

Also it is known that τ_{zx} reaches a maximum at a very small distance from crack. It has been necessary to have a very fine mesh, of 0.05 mm increments, to show the adhesive shear starting at $\tau = 0$ and reaching a maximum at $x = 0.16$ mm of 85 MPa. The procedure used in C5033 is to evaluate the margins of safety in the adhesive, using computations of maximum strain at $x = 0$. For a comparison with the F.E. the solution used by C5033, which is based on lap joint theory and assumes no bending, can be formulated in terms of the shear stress and is derived from equation (16) of ref (16):

$$\tau_{max} = \Omega_L \sigma^* G_a l / (E_1 t_a) + \Omega_T (G_a l / (E_1 t_a))(\alpha_1 - \alpha_2) \Delta T \qquad \text{...(6)}$$

The first term is due to the applied stress and the second term is due to residual thermal stress.

Also the shear stress is related to the maximum shear stress by:

$$\tau = \tau_{MAX} e^{-x/l} \qquad \text{...(7)}$$

These quantities are defined as:

31

$$l = (t_a / G_a) \left[E_1 E_0 t_1 t_0 / (E_1 t_1 + E_0 t_0) \right]^{1/2} \qquad \qquad ...(7)$$

where σ^* is the stress in the absence of a repair

E_1, t_1, α_1 are the boron modulus, thickness and coefficient of thermal expansion respectively

E_0, t_0, α_0 are the skin modulus, thickness and coefficient of thermal expansion respectively

G_a, t_a are the shear modulus and thickness of the adhesive respectively

t_1 for a single lap joint the thickness is divided by 2.

ΔT is the difference between the cure and operating temperatures

Ω_L , Ω_T parameters defined in C5033

The term Ω_L is a factor normally taken to be 1.2 . This is to cover the additional load that the repair attracts from the surrounding structure as a result of the increased stiffness. This factor can also include a bending correction term. However for comparison purposes the lap joint results and the F.E. results presented here are unfactored and the value of Ω_L is taken to be a load attraction factor only.
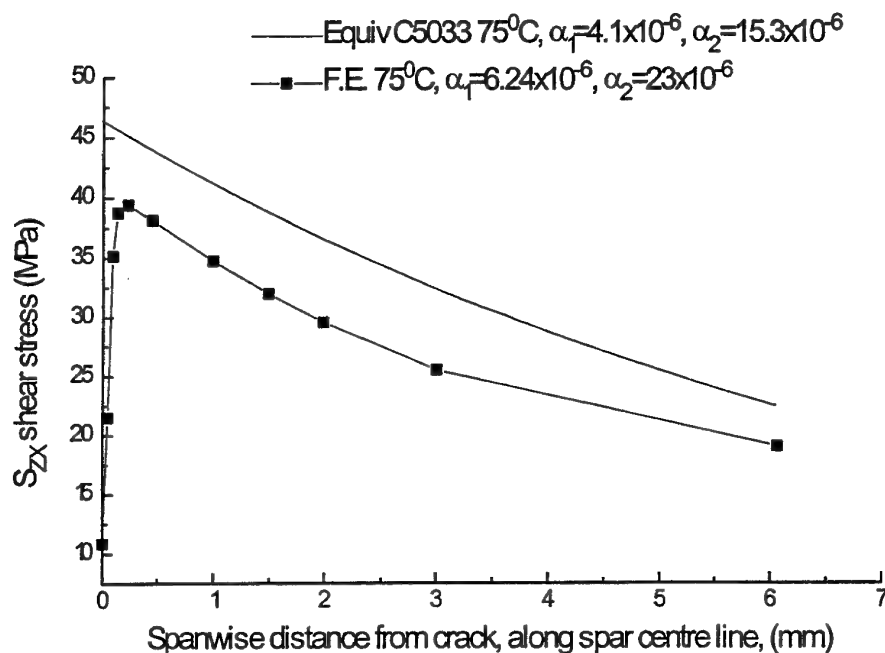

Figure 26 Adhesive shear stress (τ_{zx}) near crack, +75ºC, at DLL.

The term Ω_T is taken as a thermal inclusion factor and is taken to be 1.5, see ref (1). C5033 uses an effective coefficient of thermal expansion for the skin which is a measure of the restraint provided by the surrounding colder structure, and is given by $\alpha_e = \alpha(1+v)/2$. The equivalent C5033 result is plotted in Figure 25 and is clearly conservative compared to the 3D F.E. result. The +75°C is shown in Figure 26, and again the equivalent C5033 result is conservative. Also, in the 3D F.E. result the effective coefficient of thermal expansion for the skin material was taken to be the actual coefficient of thermal expansion for the material. This is a conservative assumption in the region of the crack since the thermal contribution increases the total shear stress. The maximum adhesive stresses provided by the linear elastic analysis indicate that the adhesive is operating in the plastic region. As previously mentioned in section 6.3 the margin of safety may be evaluated using a linear elastic analysis based on the strain energy of the adhesive taken to failure. The equivalent elastic shear stress (τ_E) based on this strain energy is shown in Table 12. Margins of safety (M.S.) have been calculated for a range of temperatures and the results are shown in Table 12. A positive M.S. exists throughout the temperature range.

Table 12 Margins of safety for adhesive in shear over crack for DUL.

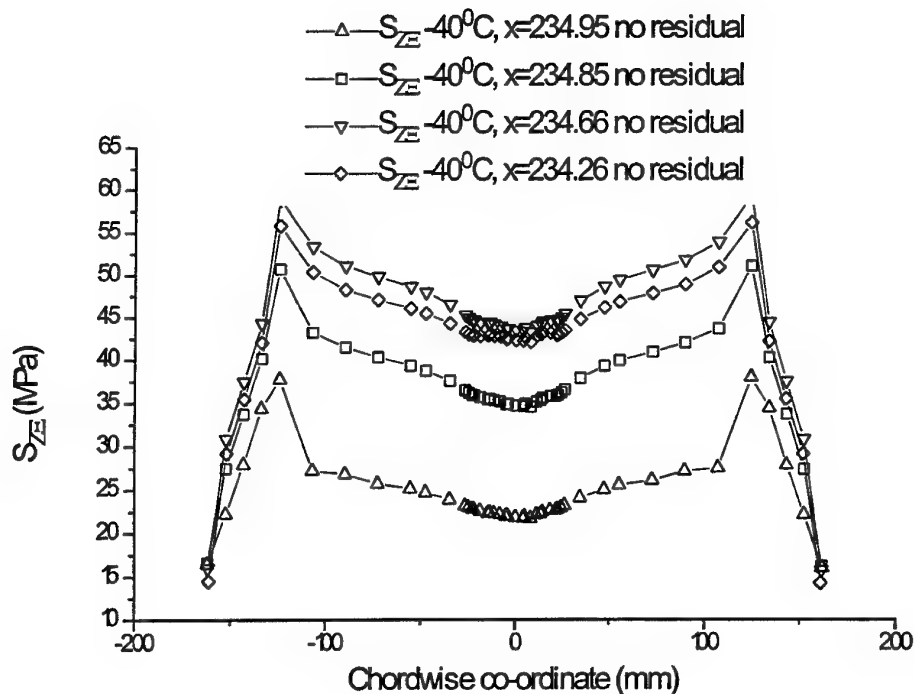| Temp	G	Strain Energy.	τ_E	τ_{3D}	M.S.
-40°C	892	22.4	199.	127.5	.561
-32°C	886	23.6	205.	127.5	.608
75°C	324	20.3	114.	58.5	.949

Figure 27. Variation of τ_{zx} in adhesive at end of patch, -40°C.

Now consider the adhesive stress state at the end of the patch, conservatively ignoring assumption made is that the contribution due to thermal residual stresses since they relieve the stresses due to flight loads at the end of the patch. Figure 27 shows the chordwise variation of the τ_{zx} midplane stresses, and corresponds to the adhesive material property state at -40°C. Figure 27 is comprised of four curves each at an increasing distance from the end of the patch. The curve having the highest value is located approximately 0.30 mm from the end of the patch. The peak value on each curve corresponds to the chamfered corner of the patch, while in comparison, the values corresponding to the forward auxiliary spar location ($y = 0$) are significantly lower. Furthermore, the peak values are superimposed on a curve which is itself higher than those values at the spar location. This suggests that bending of the unsupported skin, midway between the forward auxiliary spar and centre or front spar, is increasing the adhesive shear stress significantly.

In the case of a 3D adhesive there are components other than τ_{zx} that must be considered. The Von Mises stress is a better representation of the failure stress for the adhesive, and this distribution is shown in Figure 28. Again the peak values occur at the chamfered corners while lower values exist in the region of the forward auxiliary spar. Also, the maximum values occur approximately 0.3 mm from the end of the patch.

The corresponding curves for the adhesive at +75°C are shown in Figures 29 and 30, and are similar to the stress plots corresponding to -40°C. However for the +75°C case the stress levels are considerably reduced as a result of the lower shear modulus, and again the maximum values occur 0.3 mm from the end of the patch. Results for the -32°C case are not shown, however the shear modulus for the adhesive at this temperature is almost identical to the -40°C case.

From Figure 12a it is evident that over the complete temperature range the adhesive will not be operating in the elastic regime, particularly in the region of the chamfered corners. However, the margins of safety have been computed for operation at these temperatures and are shown in Table 13. Positive margins of safety exist throughout the temperature range. The shear stress predicted by the 1D lap-joint equation are shown in Table 14. These values are considerably lower than those predicted by the 3D F.E. analysis shown in Figures 27 & 29.

Table 13 Margins of safety for adhesive at end of patch for DUL.

Temp	G	S.S.	τ_E	$\tau = \sigma_{VM}/1.732$	M.S.
-40°C	892	22.4	199.	88.3	1.25
-32°C	886	23.6	205.	88.3	1.32
75°C	324	20.3	114.	59.5	0.92

Table 14 Shear stress predicted by lap-joint equation (MPa)

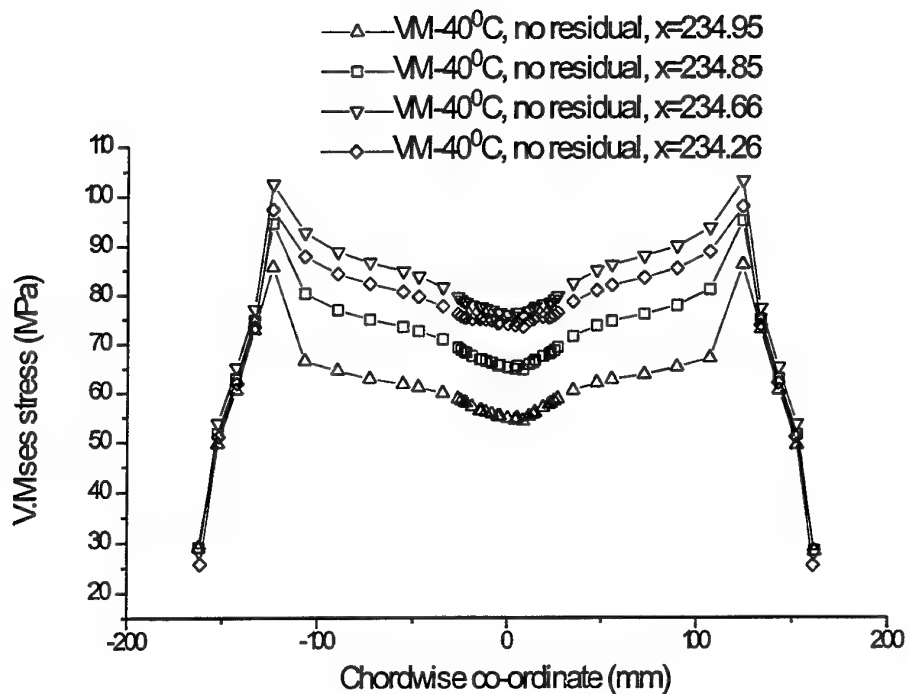| -40°C	+75°C
27.48	16.56

Figure 28. Variation of σ_{VM} in adhesive at end of patch, -40ºC.
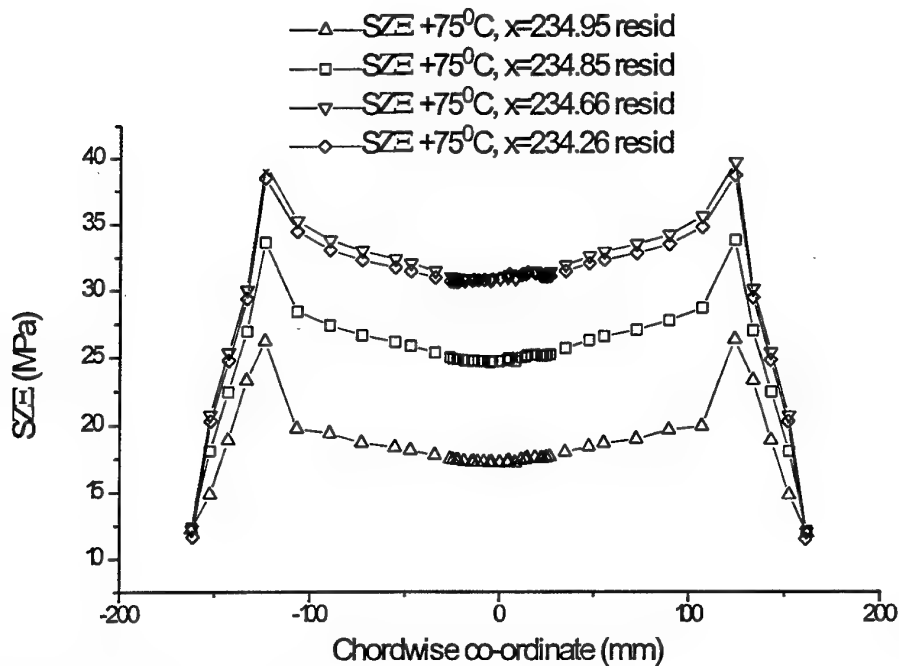

Figure 29. Variation of τ_{zx} in adhesive at end of patch, for 75ºC.
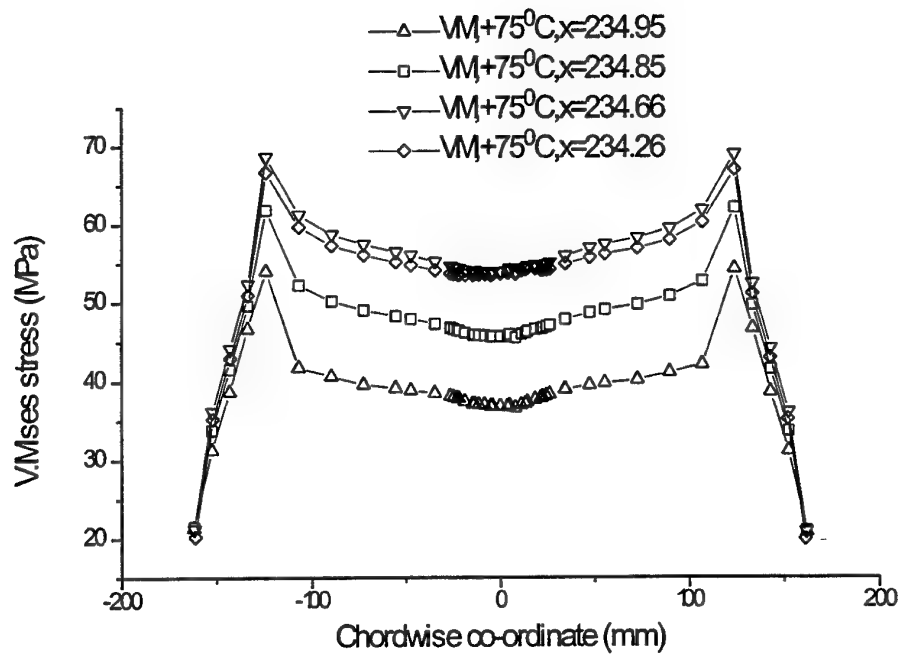
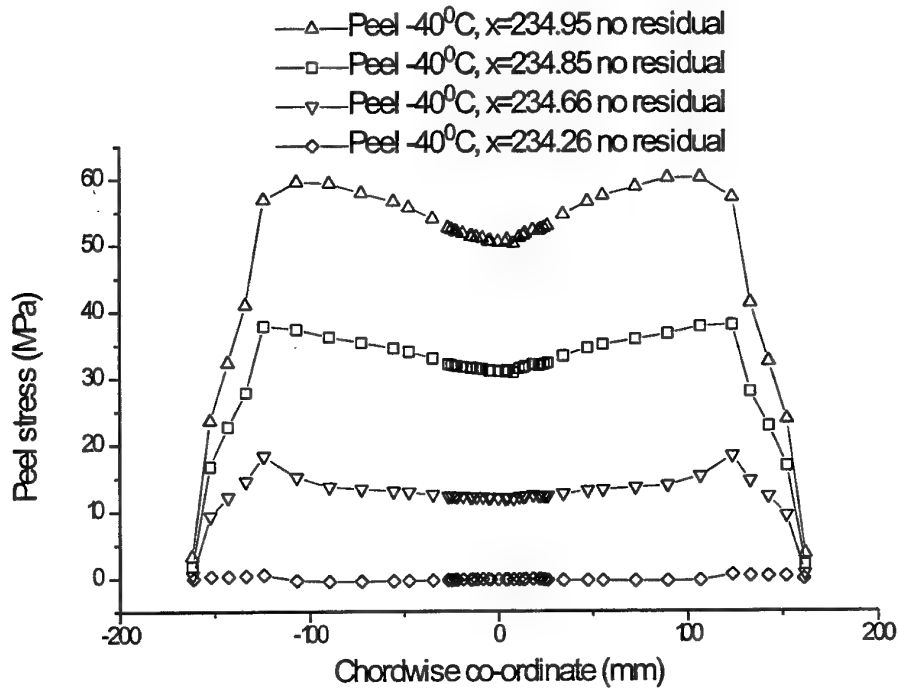*Figure 30. Variation of σ_{VM} in adhesive at end of patch, for 75°C.*

Figure 31 Variation of σ_{ZZ} in adhesive at end of patch, for -40°C.
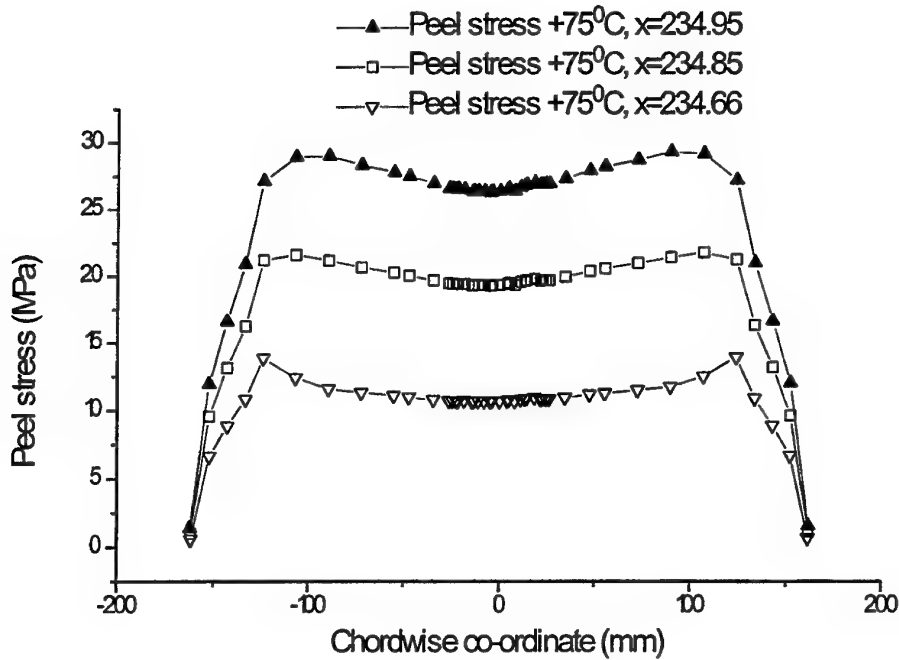
Figure 32. Variation of σ_{zz} in adhesive at end of patch, for 75ºC.

7.2.3.2 Adhesive peel stresses

The adhesive peel distribution around the end of the patch is shown in Figure 31 for the case of -40°C. Peak values occur in the region of the chamfered corner while lower values occur in the region of the spar ($y = 0$). The maximum peel stress occurs exactly at the end of the patch and decays rapidly in a distance of 0.7 mm. Also the slightly higher values away from the spar location indicate that bending of the unsupported plate has a slight influence. The peel stress distribution corresponding to adhesive material properties at +75°C are shown in Figure 32. In comparison to the -40°C case the stresses are lower simply due to the lower adhesive shear modulus at the higher temperature.

Comparisons of the F.E. are made with the d.e. expression, given by Hart-Smith, ref (12). This expression is used by C5033 and can be used for a single lap joint but with no bending:

$$\sigma_p = -w_o\, E_c/t_a \qquad \qquad ...(9)$$

where

$$w_o = (A/2)\, (e^{\chi(x-1/2)} + e^{-\chi(x+1/2)})\, \mathrm{Sin}\, \chi x$$

$$+(B/2)\, (e^{\chi(x-1/2)} - e^{-\chi(x+1/2)})\, \mathrm{Cos}\, \chi x \quad ...(10)$$

where

$\chi = (E_c/(4D\, t_a))^{0.25}$

$A = (\tau\, (t_a/2D)\, \text{Sin}\, \chi\, l/2\,) /\, \chi^3$

$B = -(\tau\, (t_a/2D)\, \text{Cos}\, \chi\, l/2)/\, \chi^3$

E_c = effective tensile modulus of the adhesive

τ = shear stress (normally taken to be the plastic value t_p)

$D = E_o\, t_o{}^3/12(1-v^2)$ and is the bending stiffness of boron

In this case the location of the coordinate system is at the midpoint of the joint, and x = ±1/2 corresponds to the ends of the joint.

A comparison of the d.e. results and F.E. work is shown in Figure 33 and 34. Again the difference between the results is substantial. Secondary bending results in very large peel stresses which exceed the allowable strength of 70mpa, ref(1), over a very small region of less than 0.5 mm diameter. While local failure of the adhesive may occur this does not mean that in this particular case that the patch itself will fail. A disbond of 6.0 mm was considered, and as a result the peel stress had reduced to that predicted by the d.e.

In deriving a solution for the d.e. for the peel it is normally assumed that the shear stress is constant. Generally this is the case when looking at the maximum strength of a bonded joint, where the adhesive is in the plastic region.
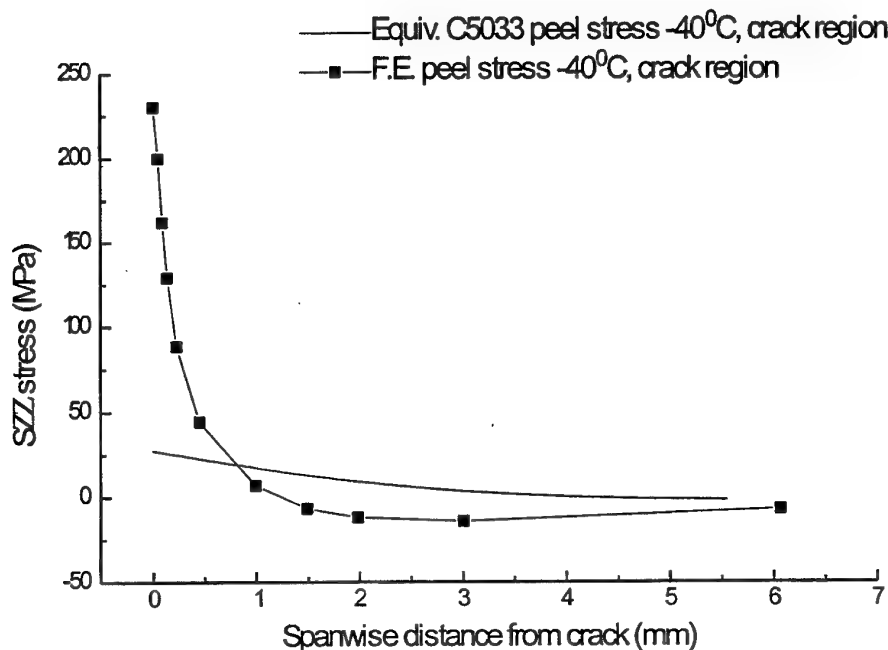

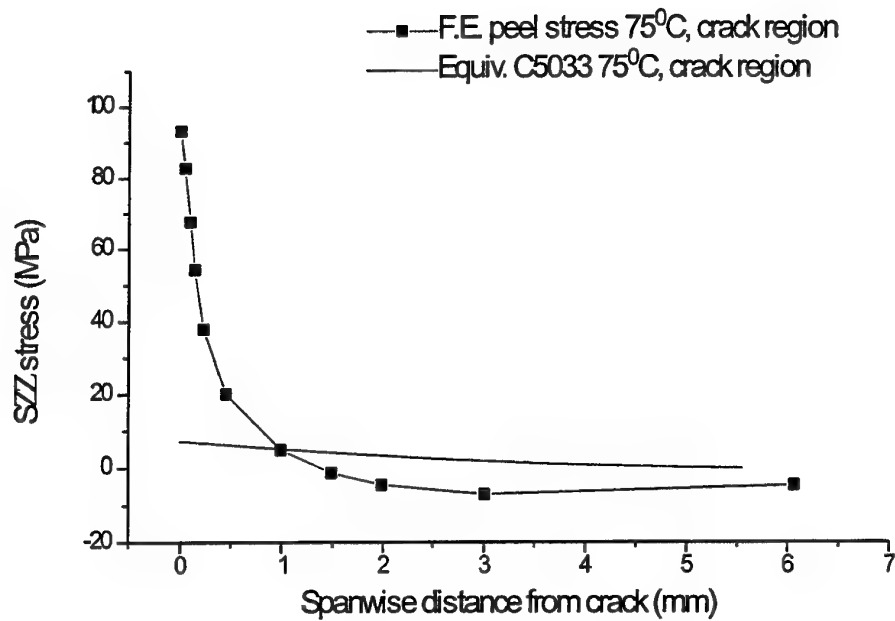Figure 33 Spanwise variation of peel stress away from crack.

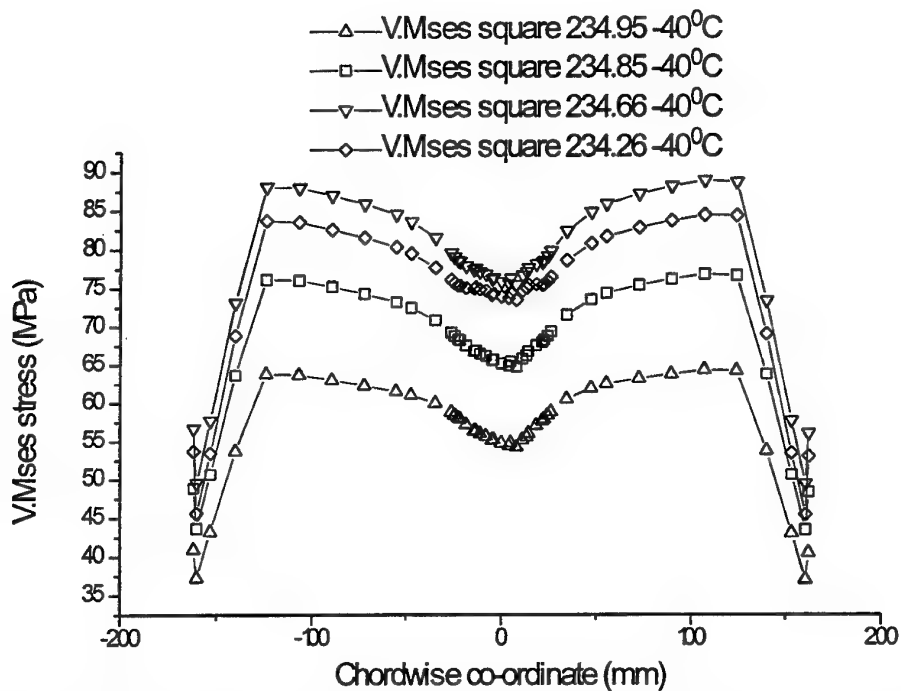*Figure 34 Spanwise variation of peel stress away from crack.*

Figure 35 Von Mises stresses at the end of the patch for square corner configuration,-40ºC.
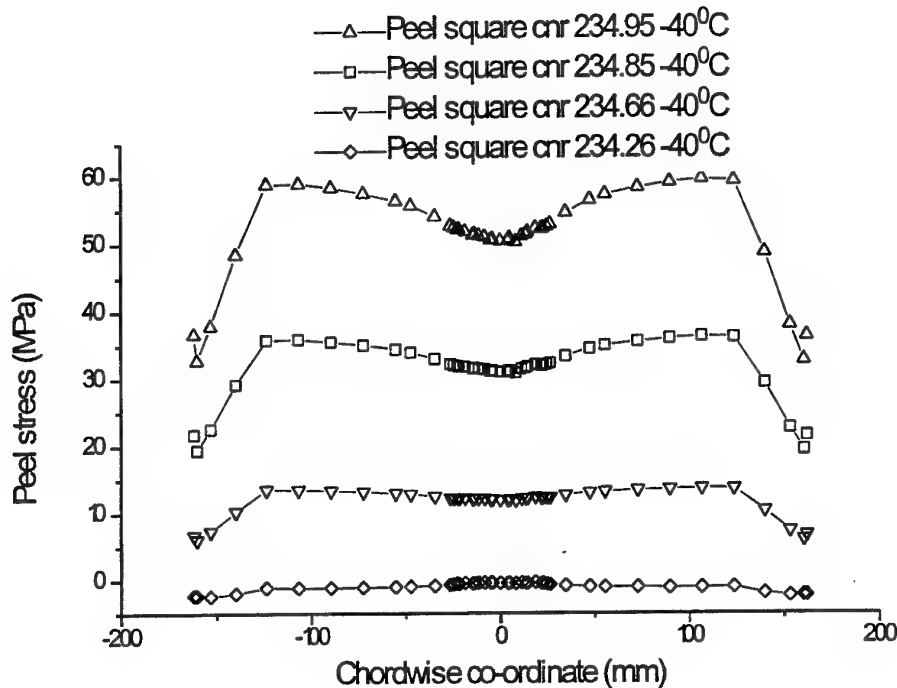
Figure 36   Variation of σ_{zz} at the end of a patch with a square corner configuration, for temperature of -40°C.

7.2.3.3   Comparison of chamfered and square corner configuration patch

A comparison has been carried out to determine the advantage of using a square patch. Figure 35 shows the Von Mises stress distribution in the adhesive corresponding to a square corner patch at -40°C, and is directly comparable to Figure 28 for the chamfered corner configuration. Given that for a 3D stress state the Von Mises stress is the best representation of failure for an adhesive, this indicates that the square corner patches may have advantages. Furthermore, it has been found in terms of stress concentration in the skin, the square corner configuration results in significantly lower stress values. In terms of peel stress, a comparison of Figures 36 and Figure 31 shows no discernible difference.

7.2.4   Boron strains

As a result of the low effective coefficient of thermal expansion in the wing skin, thermal residual stresses in the boron have not been included. Figure 37 shows the chordwise variation of the spanwise boron strains either side of the spar centre line for the lower surfaces. The dip in the strain distribution at the spar centre line indicates that secondary bending is present. These curves are similar to those shown for the uncracked case shown in Figure 13. The behaviour of the patch directly over the crack area is clearly sensitive to temperature. The minimum strains, directly over the spar for

the -40°C and room temperature case are much lower than the 75°C case. An explanation is that at 75°C the lower stiffness of the adhesive is unable to constrain the boron and less bending occurs at this point. The measured boron strains, ref (13), have been scaled up to DLL and are shown in Figure 37. The F.E. predicted strains away from the spar centre line are 10% higher than the RAAF measures strains, however the actual skin thickness of the aircraft involved is not known. To evaluate the wing skin thickness effect on these strains a wing skin thickness of 4.0 mm was considered as shown in Figure 38. The agreement with measured strains, located away from the centre line, has improved significantly. The centre gauge (gauge length of 12.5 mm) is in a region of a very high strain and when the F.E. results are averaged over the length of the strain gauge some error exists. Ultrasonic measurements of the thickness distribution in the uncracked, unpatched wing indicate that significantly more skin material has been removed in the spanwise direction than is allowed for in the drawings. As a result the spanwise strain gradient would be reduced. If this is also the case with the repaired aircraft then this would explain the error obtained at the centre gauge.

The results shown in Figure 39 correspond to spanwise strains in the boron along the spar centre line for the lower surfaces and extend to a distance of 85 mm from the crack. These strains are approximately 3000 microstrain and reach a peak at 10 mm outboard of the crack along the spar centre line. Results shown in Figure 40 correspond to the upper surface strains whose peak values are approximately 11,000 microstrain directly over the crack, at DLL. In this region two elements have been used through the thickness of the boron, and as a result the predicted strains are considered to be accurate. These strains are considerably higher than those obtained in the uncracked case shown in Figure 15. It is likely that this increase is due to the change of the load path in the region of the crack. The load is now carried by the boron and the neutral axis offset has been increased, resulting in increased bending of the boron.

It has been shown previously that the peel stresses in the adhesive in the region of the crack will result in local failure. A representative test article, used in the structural testing program, has shown disbonds of approximately 5 mm either side of the crack under representative loads. A 6 mm disbond has been included in a F.E. model, and the corresponding boron strains are shown in Figure 41. The highest strains occur 5 mm away from the crack and are approximately 4500 microstrain. It is likely that the plasticity of the adhesive at the disbond will reduce these strains and the maximum values considered are those occurring over the crack. The disbond has also reduced the magnitude of the lower surface strains for both -40°C and 75°C temperatures.

Maximum strains in the boron for the required temperature range and margins of safety are shown in Table 13.
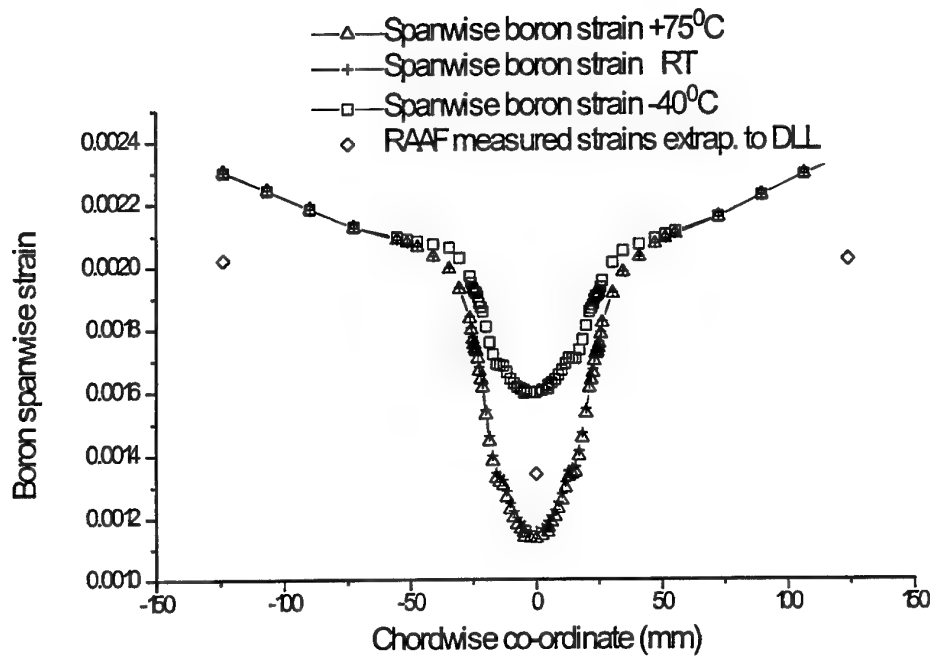
Figure 37 Spanwise lower surface boron strain in plane of crack for -40ºC, room temperature and 75ºC cases.
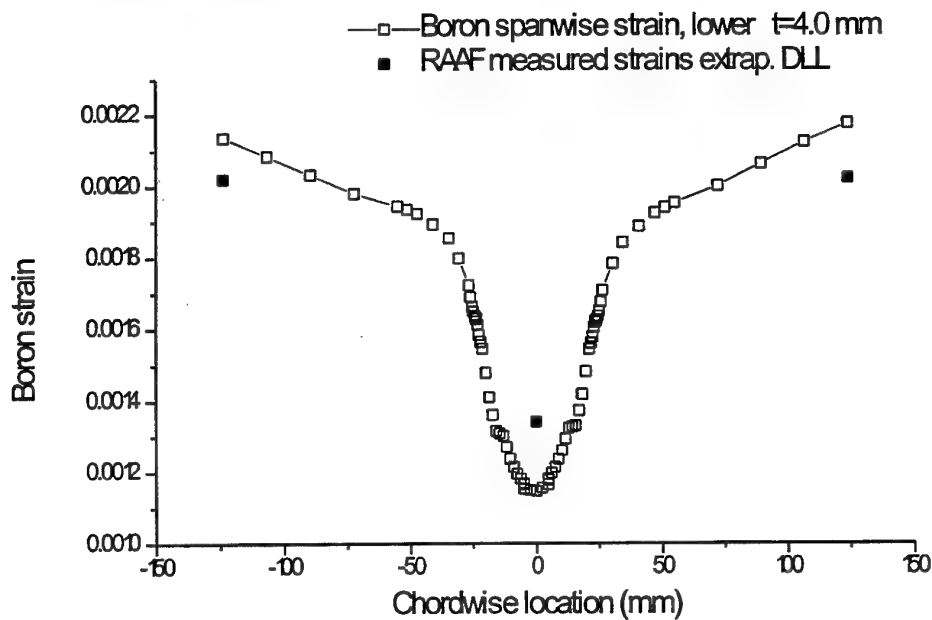
Figure 38 Spanwise lower surface strain in plane of crack for -40ºC corresponding to a skin thickness of 4.0 mm.
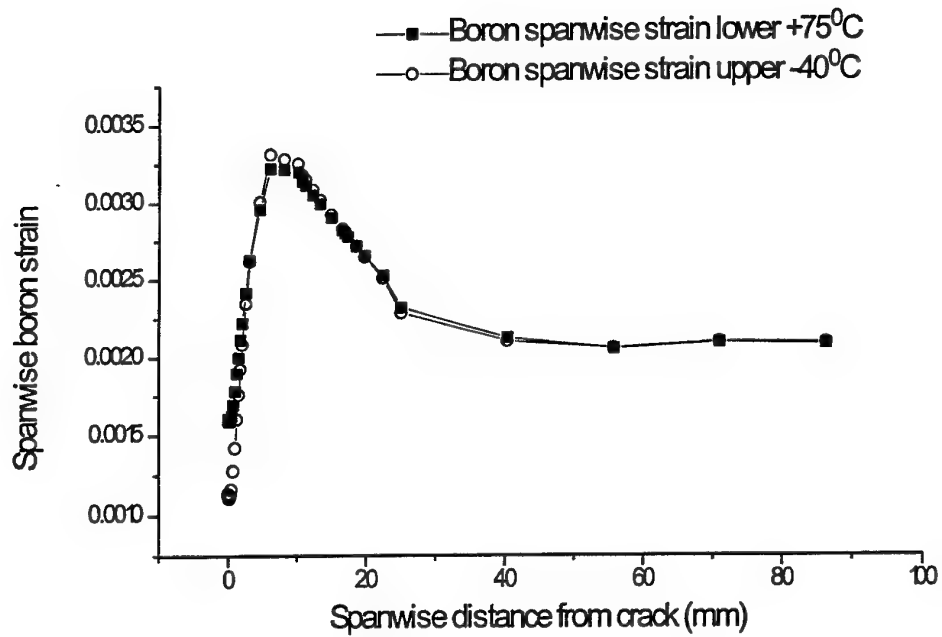
Figure 39 Spanwise boron lower surface strain for 48mm crack.
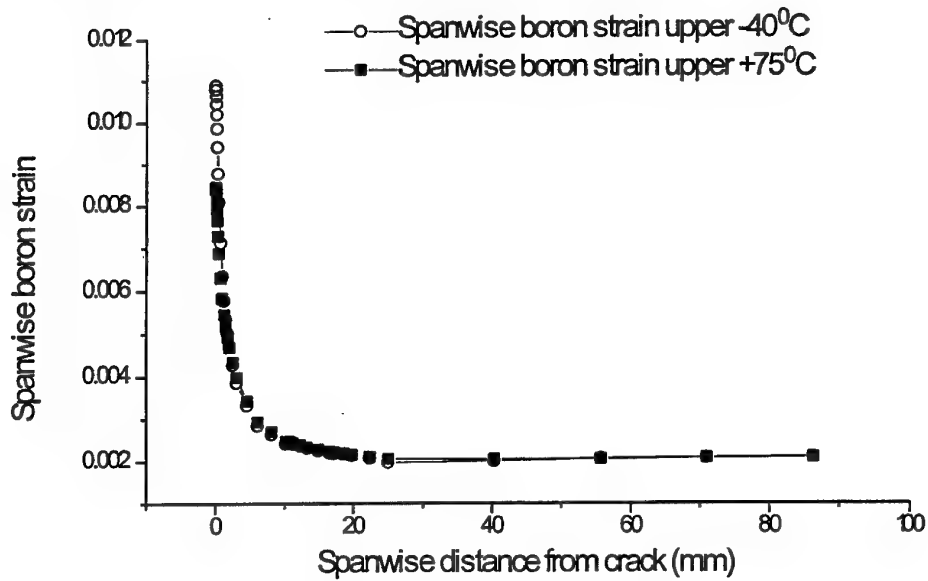
Figure 40 Spanwise boron upper surface strain for 48 mm crack.
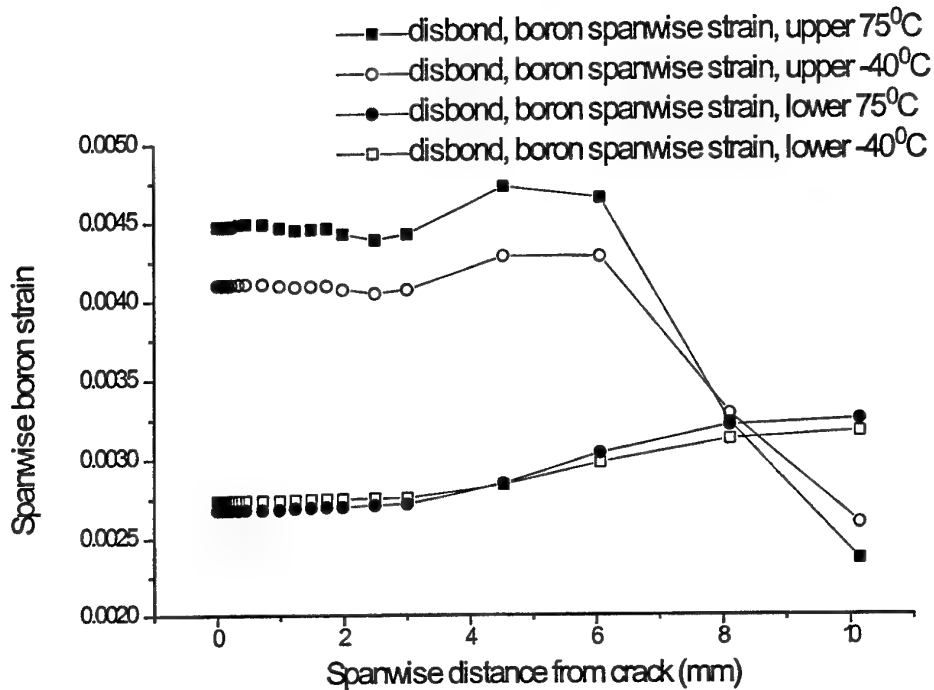
Figure 41 Disbond, variation of spanwise upper surface boron strain with distance from crack.

Table 15. Margins of safety in boron at DUL.

Temperature ⁰C	Maximum allowable strain	Ultimate strain	m.s.
-40	6000.	6150.	-.024
-32	6000.	6150.	-.024
+75	6000.	6750.	-.111

7.2.5 Boron interlaminar shear

Graphically, the maximum interlaminar shear stresses have been found to occur over the crack. The allowables are given in Table16, together with the maximum values in the repair at DUL. The margins of safety are positive throughout the temperature range.

Table 16 Interlaminar shear in region of crack

Temperature ⁰C	Allowable Int. shear (MPa)	Interlaminar shear (MPa)	m.s.
-40	97	41.16	1.36
-32	97	41.16	1.36
+75	55	22.2	1.48

8. Comparison of C5033 and 3D F.E.

8.1 Source of equations used in RAAF design

The following formulae used for patch design, have been compared with the results of the 3D F.E. . While the derivation of these equations will not be carried out, where possible the source of these equations will be identified.

8.1.1 Stress in the skin under the repair

Following is the equation for the direct stress in the skin under the repair:

$$\sigma_o = \Omega_L \sigma / (1+s) + \Omega_T E_1 s / (1+s))(\alpha_1 - \alpha_2)|\delta T| \qquad \text{...(11)}$$

where $s = E_o t_o / (E_1 t_1)$ ...(12)
$\Omega_L = 1.44$
$\Omega_T = 1.5$

This equation is derived from equilibrium considerations and is made up of 2 terms. The first term identifies the stress level in the skin resulting from load transfer into the region, while the second term is a result of the thermal stress. Normally the load attraction factor $\Omega_L = 1.2$. In this case however, two correction factors have been applied to Ω_L. One is due to the increased load the patched structure attracts, due to increased stiffness. The other is caused by a stress concentration due to bending effects, the derivation of which is included in ref (1). Consider now the second term of equation (11). This is the direct stress in the skin as a result of thermal stress/residual stress, and is derived from equation (6.1a) of ref (17). Also, this term contains a correction factor of $\Omega_T = 1.5$, . Thermal stresses may be considered to be bi-directional in the plane of the adhesive, and hence some stress concentration factor is appropriate for bending effects.

8.1.2 Maximum adhesive shear strain

The expression for maximum adhesive shear strain is based on simple lap joint theory which has been extended to include plastic deformation. The first step used in ref (1) was to compute the shear strain which defines the elastic limit. This equation is derived from equation (5.26) of ref (16), and is given by:

$$\gamma_{max} = \sigma_0 t_1 \lambda / G_a \qquad \text{...(13)}$$

If this exceeds the elastic limit for the adhesive shear strain, then the plastic limit must be computed and is derived from equation (5.27) of ref (16) and is given as:

$$\gamma_{max} = \left(\tau_p / (2G_a)\right)\left[1 + \left(\sigma_0 t_1 \lambda / \tau_p\right)^2\right] \qquad \text{...(14)}$$

where the parameter λ, is given by equations (5.9) of ref (16) as:

$$\lambda = \left[\left(G_a / t_a\right)\left[1 / \left(E_1 t_1\right) + 1 / \left(E_0 t_0\right)\right]\right]^{1/2} \qquad \text{...(15)}$$

where the elastic transfer length is given by $1 / \lambda$.

Essentially, the margin of safety is based on the computation of available energy calculated as the area under the adhesive stress strain curve taken to failure.

8.1.3 Stress intensity in the repaired skin

The stress intensity in the repaired structure is a function of the stress in the skin under the patch, and other patch parameters. The concept of an upper bound for K_∞, which is independent of crack length, was derived from equations (5.22) and (5.28) developed in ref (16) and is given by:

$$K_\infty = \left[\left(E_1 t_a / G_a\right)\left(\sigma_0 \tau_P K_2 - \tau_P^2 K_1 / \left(\lambda t_1 3\right)\right)\right]^{0.5} \qquad \text{...(16)}$$

where $K_1 = 1 + 2\left(\sigma_0 t_1 \lambda / \tau_P\right)^3$ $\qquad \text{...(17)}$

and $K_2 = 1 + \left(\sigma_0 t_1 \lambda / \tau_p\right)^2$ $\qquad \text{...(18)}$

The results shown in Figure 13 which correspond to the skin/spar patched results, indicates that the value of K_1 is constant and independent of crack length.

8.1.4 Adhesive peel stresses

The derivation of the maximum peel stress is given by equation (83) of ref (12) as a function of the shear stress:

$$\sigma_{max} = \tau_P \left[3E_C^i t_0 (1 - v^2) / (E_0 t_a)\right]^{0.25} \qquad \text{...(19)}$$

where E_C^i is the effective transverse tensile modulus of the adhesive and is given by equation (68) of ref (12) as:

$$E_C^i = \left(1 / E_C + 2 / E_1 + 4 / E_0\right)^{-1} \qquad \text{...(20)}$$

The value of τ_p is taken to be the ultimate failure strength of the adhesive. The calculation of the peel stresses have been evaluated in the region of the crack and at the end of the patch.

8.1.5 Maximum stress in patch

The maximum direct stress is derived from simple equilibrium considerations in which no bending occurs and is given by:

$$\sigma_p = \sigma t_1 / t_o \qquad \qquad ...(21)$$

This formulae is only applicable to the region directly over the crack. Computations of interlaminar shear for Boron/epoxy are not considered.

8.1.6 Strength properties

A summary of ultimate strength properties obtained from ref (1) is shown in Table 8. The M.S. derived from F.E. results are based on these strengths.

Table 17 Strength properties of skin, boron/epoxy and adhesive.

	Temperature	Temperature	Temperature
Parameter	-40°C	-32°C	75°C
Skin ultimate strength in the rolling direction 2024-T851 (MPa)	448	448	448
Skin fracture toughness K_{IC} ($MPa\sqrt{m}$)	46.2	46.2	46.2
Adhesive shear strain γ_E	.0903	.0866	.067
Adhesive strain shear γ_P	.4377	.486	1.493
Adhesive peel stress (MPa)	70.0	70.0	70.0
Boron laminate ultimate strain γ	.006	.006	.006

The values shown in Table 17 are derived from the RAAF design package, ref(1), and rely on:

1. 2024-T851 Properties from ref (5)
2. Fracture toughness tests at AMRL
3. FM73 Manufacturer's data, ref (11)
4. Boron Manufactures data, ref (9)

The peel strength allowable of 70 MPa, ref(1), used throughout the temperature range, is open to question. Data for FM73 at room temperature (RT), from ref(19), gives an ultimate tensile strength of 44.2 MPa and is taken to be the ultimate peel strength. Unfortunately data does exist for other temperatures. Simple ratios have been found to exist between shear yield and tensile yield for epoxy adhesives in refs(20) and (21). Extending this to ultimate strengths and using data from Figure 12 and 42, some

approximate peel strengths have been computed as shown in Table 18. (The shear strengths for -40°C and -32°C are assumed to be approximately the same as the -55°C case). These peel strengths are based on a ratio of peel/shear ratio of 44.2/40 and are derived from the RT data. While the RT ultimate strength is 44.2 MPa, the equivalent elastic failure strength based on the same strain energy to failure is 55.4 MPa, as shown in figure 42. A further factor of (55.5/44.2) is applied to the ultimate peel strengths to obtain the equivalent elastic allowable, and is shown in Table 18. There is clearly, a need for temperature dependent peel stress data for FM73.

Table 18. Estimated peel strength variation with temperature (also includes RT data)

Temperature °C	-40	RT	+75
Estimated peel strength (MPa)	63.5	44.2	37.2
Equivalent Elastic allowable (MPa)	81.6	55.5	46.8

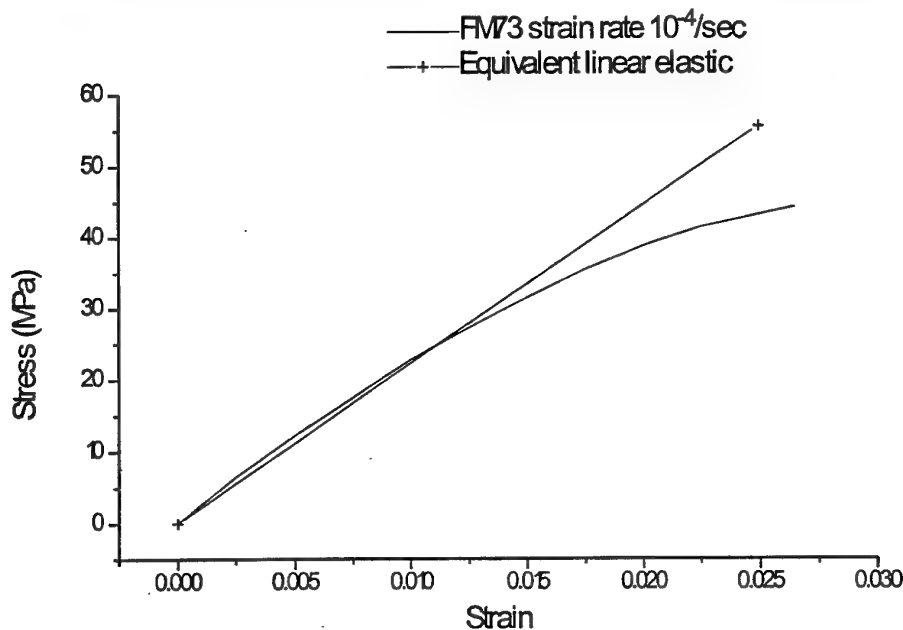*Figure 42 Tensile stress strain curve for FM73 at room temperature and at a strain rate of 10⁻⁴/sec, from ref(19).*

8.2 Summary of 3D F.E. stress/strain results

A summary of the 3D F.E. results are shown in Table 18.

8.2.1 Skin

The F.E. analysis confirmed that the repaired structure containing a 48 mm crack has a positive M.S. at DUL, based on a fracture toughness value (K_{IC}) of 46 MPa$\sqrt{m}$.

Furthermore the associated testing program has confirmed the value of K_{IC} . The margin of safety at +75°C is slightly higher than at the lower temperatures, mainly as a result of the lower thermal residual stress. The analysis has also confirmed that a positive M.S. exists at DUL for the stress in the skin throughout the operating temperature range.

8.2.2 Adhesive

8.2.2.1 Adhesive shear

The maximum shear stresses for the -40°C case have been found to be near the crack region, while for the +75°C case the stresses at the chamfered corner are equal to those near the crack region.

8.2.2.2 Adhesive peel

The maximum peel stresses occur at the crack, and are caused by large out of plane displacements. While local failure will occur near the crack over a very small region, this failure will not spread. The important peel stresses are those at the end of the patch since failure in this region will result in complete failure of the patch. M.S. are based on approximate data and failure at the lower temperatures is close to the DUL.

8.2.3 Boron

8.2.3.1 Maximum strains

The maximum strains occur over the crack region of the upper surface of the boron, and is equal to 12000 microstrain at DLL. However a disbond is expected to form in this area before DLL is reached. The maximum expected strain in the boron at DUL, after a disbond, is 6750 microstrain. The maximum lower surface strains occur a distance of 10 mm away from the crack is equal to approximately 3800 microstrain. A small negative M.S. occurs throughout the temperature range.

8.2.3.2 Interlaminar shear

The maximum interlaminar shear stress occurs over the crack region and a positive M.S. exists throughout the operating temperature range.

Table 18. A summary of the 3D F.E. results at DUL

Parameter	-40ºC	-32ºC	75ºC
Skin: Stress intensity factor (patched) ($MPa\sqrt{m}$)	26.68x1.5=40.0	26.68x1.5=40.0	25.10x1.5=37.7
Adhesive: Shear over crack.(MPa)(Table 12)	1.5x118. = 153.	1.5x118. = 153.	1.5x67.= 103.
Adhesive: Peel over crack(MPa)	230x1.5 = 345.	230x1.5 = 345.	87x1.5 = 131.
Adhesive: Von Mises at end of patch. (MPa)(Table 13)	1.5x1.732x88.3 = 229.4	1.5x1.732 x88.3= 229.4	1.5x1.732 x59.5= 154.6
Adhesive: Peel at end of patch (Fig. 30,31)	59.3x1.5=88.95	59.3x1.5=88.95	29.2x1.5=43.8
Boron: Direct strain over crack (Table 15)	1.5x4100 = 6150.u	1.5x4100 = 6150u	1.5x.4500=6750 .u
Boron: direct strain at end of patch	1.5x1730 = 2595u	1.5x1730= 2595u	1.5x2930= 4395u
Boron: Inter-laminar shear. stress adjacent to crack (Table 16)	approx 1.5x27.44 = 41.16 MPa	41.16 MPa	approx 1.5x14.8 = 22.20 MPa
Boron: Inter-lam. shear stress at end of patch	approx 1.5x12. = 18.0 MPa	approx 1.5x12. = 18.0 MPa	approx 1.5x8.89 = 13.33 MPa

8.3 Comparisons of margins of safety

The overall results are shown in Table 18. A comparison of the results from the F.E. analysis and results predicted by C5033, are shown in Table 19. Note that the M.S. originally calculated by the RAAF in ref (1) correspond to DLL. The following values have been re-calculated and now correspond to DUL.

8.3.1 Stress intensity factor

A small difference is noted between the M.S. for stress intensity factor predicted by F.E. and C5033. The F.E. results show a lower M.S. for K_I at the lower temperatures and is due to lower residual thermal stress experienced. However, at a temperature of +75°C the M.S. is higher.

8.3.2 Adhesive shear

8.3.2.1 Over crack

The M.S. for adhesive shear over the crack predicted by the F.E. method is higher, and is largely due to the conservative value used for Ω_T in ref (1).

8.3.2.2 End of patch

The M.S. for adhesive shear at the end of the patch is not computed in ref (1), since it is assumed that the critical shear values occur in the region of the crack.

8.3.3 Adhesive peel

The M.S. for adhesive peel predicted by the F.E. method at the end of the patch is significantly different, since peel stress failure data used is dependent on temperature.

8.3.4 Boron strain

The M.S. predicted by the F.E. for the boron strain is substantially lower and is due to bending in the region of the crack, as a result of the neutral axis offset. The F.E. is conservative because it did not take into account the thermal residual compression strain which is beneficial.

8.3.5 Overall M.S.

While some disagreement occurs over the values of M.S. it is clear that the structural integrity of the RAAF designed repair is confirmed.

Table 19. Comparison of m.s. predicted by C5033 and 3D F.E. for 48 mm crack at DUL.

	C5033	C5033	C5033	3D F.E.	3D F.E.	3D F.E.
Parameter	-40° C	-32°C	75° C	-40° C	-32°C	75° C
Skin: Stress intensity factor (patched)	0.227	0.087	0.019	.155	.155	.225
Adhesive: Shear over crack. Table 10	0.448	0.399	1.581	0.561	0.608	0.949
Adhesive: Peel over crack	-	-	-	*	*	*
Adhesive: shear at end of patch. (Von Mises) Table 11	-	-	-	1.25	1.25	0.92
Adhesive: peel at end of patch	0.349	0.390	5.271	-.083	-.083	.068
Boron: direct strain over crack	0.610	0.359	0.359	-0.024	-0.024	-0.111
Boron: direct strain at end of patch	-	-	-	0.092	0.093	0.128
Boron: Inter-lam. shear stress adjacent to crack	-	-	-	1.36	1.36	1.48
Boron: Inter-lam. Shear stress at end of patch	-	-	-	4.39	4.39	3.13

* failure limited to a small region

9. Conclusions

A 3D F.E. model of the skin/spar structure has been developed and validated with strain gauge data from a full size uncracked wing. The 3D F.E. model has been extended to model the fatigue crack, the RAAF designed boron fibre patch and refined to the extent necessary to evaluate adhesive parameters. Furthermore strain gauge readings made by the RAAF on the repaired wing have also validated the F.E. model with the composite repair.

Stress intensity factors have been evaluated for a range of crack lengths for the unrepaired and repaired structure, and the crack growth rate is expected to be reduced by a factor of 100, and is in agreement with test results.

The reduction of the maximum stress occurring in the upper surface of the skin for the uncracked, patched configuration to the yield stress value, corresponding to a 3.6 mm skin, indicates that there may be a case for patching the complete fleet of F-111 aircraft.

Comparisons made between simple lap joint formulae indicate that secondary bending can increase the adhesive shear and peel stresses. However, the bending correction factors used in the original design were adequate. The differences in m.s. between the 3D F.E. and the closed form solutions are not significant.

While a comparison of the Von Mises adhesive stresses at the ends of the patch has shown that a configuration with square corners may have advantages, a high M.S. exists at this location.

The Von Mises stresses in the skin are lower with the square corner configuration, however this is not significant.

Not only has 3D F.E. confirmed the structural integrity of the RAAF designed boron/epoxy patch at DUL, but also the use of those equations in C5033 at the time of the design.

10. Acknowledgments

11. References

1. Anon Design approval package for the bonded repair to aircraft A8-145., 1994.

2. Anon. RAAF Engineering Standard C5033. Composite Materials and Adhesive Bonded Repairs.

3. Keeley, D, Callinan, R.J, and Sanderson, S., "Validated Finite Element Model of an F-111 Lower Wing Skin Structural Detail at Forward Auxiliary Spar Station (FASS) 281.28.", DSTO-TN-0046, Aug. 1996.

4. Anon General Dynamics drawings 12W951.

5. Anon. MIL-HDBK-5F Metallic Materials and Elements for Aerospace Structures 1 Nov. 1970.

6. Watters, K F-111 Outer Wing Strain Survey at fuel flow hole in the forward auxiliary spar. Structures Laboratory report. 1/94. 15.9.94

7. Williams, J.F., Jones, R. and Goldsmith, N. An introduction to Fracture Mechanics. Theory and case studies. Trans. Inst. Engs. Aust. ME 14, No.4,1989.

8. Gdoutos, E.E. Fracture Mechanics. An introduction. Kluwer Academic. 1993.

9. Anon. 5521/4 Boron/Epoxy Prepreg Tape (250⁰F Cure) Textron Specialty Materials.

10. Hadcock, R.N. Table 24.3, 'Boron-Epoxy Aircraft Structures', Handbook of Fiberglass and Advanced Plastics Composites. Van Nostrand Reinhold, 1969.

11. Anon FM73 Film adhesive. Manufactures data. Table IV. CYTEC Corporation.

12. Hart-Smith, L.J., "Adhesive-Bonded Double-Lap Joints." NASA CR 112235, Jan. 1973.

13. Wilkin, M.O. F-111 A8-145 Lower Wing Skin Crack Strain Survey. ASI/4060/6/A8/3 (4). 13 Sept. 1994.

14. Baker, A.A., Hawkes, G.A. and Lumley, E.J., 'Fibre Composite Reinforcement of Cracked Structures - Thermal - Stress and Thermal - Fatigue Studies', ICCM2 Proceedings of the 1978 International Conference on Composite Materials. Editors: B. Noton, R. Sigorelli, K. Street and L. Phillips. April 1978 Toronta, Canada.

15. L. Mirabella. Strain gauge and temperature measurements of a heated F-111 wing.

16. Callinan, R.J., Sanderson, S, Tran-Cong, T. and Walker, K. Development and Validation of a Finite Element Method to Determine Thermally Induced Stresses in Bonded Joints of Dissimilar Materials. Draft.

17. Rose, L.R.F., 'Theoretical analysis of crack patching'. Edit. Baker, A.A. and Jones, R. Martinus Nijhoff,1988.

18. Baker, A.A. Crack patching: experimental studies, practical applications. 'Bonded Repair of Structures.' Edit. A.A. Baker and R. Jones.

19. Chalkley, P. A Critical Compendium of Material Property Data for Bonded - Composite Repairs. Draft report, 1996.

20. Callinan, R.J. and Paul, J.J. Bonded repairs of Metallic Aircraft Components Damaged by Corrosion. ARL-TR-46, Nov 1993.

21. Raghava, R., Caddell, R.M. and Yeh, G.S.Y. 'The macroscopic yield behaviour of polymers' J.Mat.Sc 8 p225-232, 1973.

Finite Element Analysis of an F-111 Lower Wing Skin Fatigue Crack Repair

R.J. Callinan, S. Sanderson and D. Keeley

AUSTRALIA

DEFENCE ORGANISATION

Task Sponsor DTA

S&T Program
Chief Defence Scientist   ⎱
FAS Science Policy   ⎰ shared copy
AS Science Industry and External Relations   ⎱
AS Science Corporate Management   ⎰
Counsellor Defence Science, London (Doc Data Sheet)
Counsellor Defence Science, Washington (Doc Data Sheet)
Director General Scientific Advisers and Trials/Scientific Adviser Policy and Command (shared copy)
Navy Scientific Adviser (3 copies Doc Data Sheet and 1 copy distribution list)
Scientific Adviser - Army (Doc Data Sheet and distribution list only)
Air Force Scientific Adviser
Director Trials

Aeronautical and Maritime Research Laboratory
Director

Electronics and Surveillance Research Laboratory
Director

Chief of Airframes and Engines Division
F. Rose
K. Walker
R.J. Callinan
S. Sanderson
D. Keeley

DSTO Library
Library Fishermens Bend
Library Maribyrnong
Library DSTOS (2 copies)
Australian Archives
Library, MOD, Pyrmont (Doc Data sheet only)

Forces Executive
Director General Force Development (Sea) (Doc Data Sheet only)
Director General Force Development (Land) (Doc Data Sheet only)

Army
ABCA Office, G-1-34, Russell Offices, Canberra   (4 copies)

Air Force
Wing Commander E. Wilson, OICASI, HQLC, RAAF Williams, Laverton, VIC
Flight Lieutenant S. White, SRLMSQN, RAAF Amberley, QLD
Mr M. Davis ATS1A, 501 Wing, RAAF Amberley, QLD

S&I Program
Defence Intelligence Organisation
Library, Defence Signals Directorate (Doc Data Sheet only)

B&M Program (libraries)
OIC TRS, Defence Central Library
Officer in Charge, Document Exchange Centre (DEC), 1 copy
*US Defence Technical Information Center, 2 copies
*UK Defence Research Information Centre, 2 copies
*Canada Defence Scientific Information Service, 1 copy
*NZ Defence Information Centre, 1 copy
National Library of Australia, 1 copy

UNIVERSITIES AND COLLEGES

Australian Defence Force Academy
  Library
  Head of Aerospace and Mechanical Engineering
Senior Librarian, Hargrave Library, Monash University
Librarian, Flinders University

OTHER ORGANISATIONS

NASA (Canberra)
AGPS

OUTSIDE AUSTRALIA

ABSTRACTING AND INFORMATION ORGANISATIONS
INSPEC: Acquisitions Section Institution of Electrical Engineers
Library, Chemical Abstracts Reference Service
Engineering Societies Library, US
Materials Information, Cambridge Scientific Abstracts, US
Documents Librarian, The Center for Research Libraries, US

INFORMATION EXCHANGE AGREEMENT PARTNERS
Acquisitions Unit, Science Reference and Information Service, UK
Library - Exchange Desk, National Institute of Standards and Technology, US
National Aerospace Laboratory, Japan
National Aerospace Laboratory, Netherlands

SPARES (10 copies)

Total number of copies   60

DEFENCE SCIENCE AND TECHNOLOGY ORGANISATION DOCUMENT CONTROL DATA	1. PRIVACY MARKING/CAVEAT (OF DOCUMENT)

2. TITLE Finite Element Analysis of an F-111 Lower Wing Skin Fatigue Crack Repair	3. SECURITY CLASSIFICATION (FOR UNCLASSIFIED REPORTS THAT ARE LIMITED RELEASE USE (L) NEXT TO DOCUMENT CLASSIFICATION) Document (U) Title (U) Abstract (U)

4. AUTHOR(S) R.J.Callinan, S.Sanderson and D.Keeley	5. CORPORATE AUTHOR Aeronautical and Maritime Research Laboratory PO Box 4331 Melbourne Vic 3001

6a. DSTO NUMBER DSTO-TN-0067	6b. AR NUMBER AR-009-961	6c. TYPE OF REPORT Technical Note	7. DOCUMENT DATE January 1997

8. FILE NUMBER M1/9/169	9. TASK NUMBER 94/118	10. TASK SPONSOR AIR	11. NO. OF PAGES 55	12. NO. OF REFERENCES 21

13. DOWNGRADING/DELIMITING INSTRUCTIONS None	14. RELEASE AUTHORITY Chief, Airframes and Engines Division

15. SECONDARY RELEASE STATEMENT OF THIS DOCUMENT

Approved for Public Release

OVERSEAS ENQUIRIES OUTSIDE STATED LIMITATIONS SHOULD BE REFERRED THROUGH DOCUMENT EXCHANGE CENTRE, DIS NETWORK OFFICE, DEPT OF DEFENCE, CAMPBELL PARK OFFICES, CANBERRA ACT 2600

16. DELIBERATE ANNOUNCEMENT

No limitations

17. CASUAL ANNOUNCEMENT	Yes

18. DEFTEST DESCRIPTORS

Finite element analysis, Bonded composite repairs, F-111 aircraft

19. ABSTRACT
In this report a three dimensional finite element (F.E.) model has been developed for a structural detail in an F-111 lower wing skin. The location of interest is a fuel - flow groove in the lower wing skin where cracking had occurred in service on aircraft A8-145. Detailed models were developed for (i) un-cracked structure; (ii) the cracked structure and (iii) the repaired structure, using a bonded composite patch for the repair. The objective of this work is to validate the design analysis used by the RAAF, using an independent approach for the stress analysis. The F.E. model has been validated using strain gauge results from a full scale test wing. The results of the F.E. analysis are shown to compare favourably with closed form solutions used by the RAAF (RAAF Engineering Standard C5033) in the original design of the repair. Thus the present work provides a basis for confidence in the design procedures contained in RAAF Engineering Standard C5033.